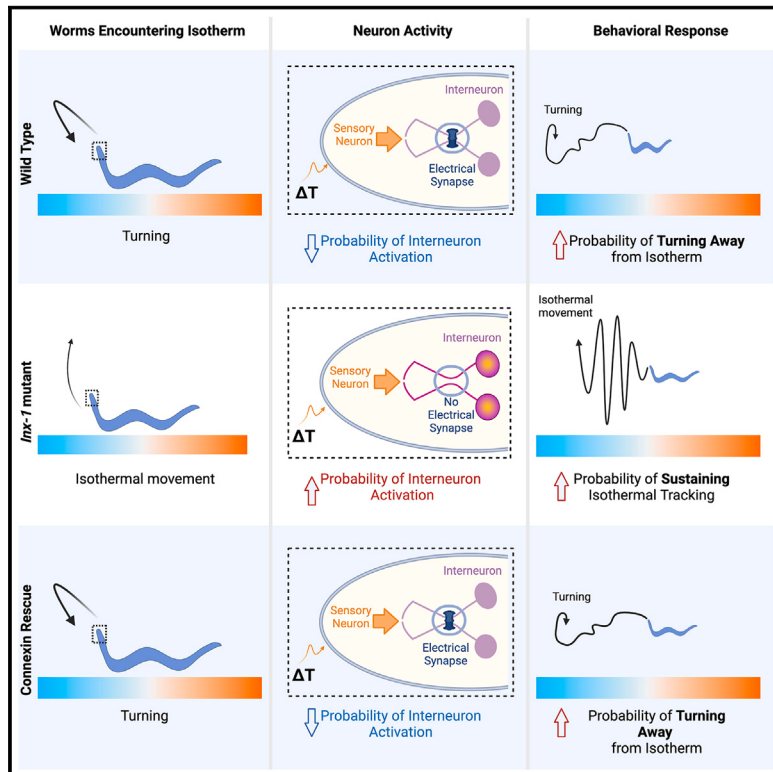


Configuration of electrical synapses filters sensory information to drive behavioral choices

Graphical abstract



Authors

Agustin Almoril-Porras, Ana C. Calvo, Longgang Niu, ..., Ivy Ren, Zhao-Wen Wang, Daniel A. Colón-Ramos

Correspondence

daniel.colon-ramos@yale.edu

In brief

Sensory information can be differentially processed, enabling *similar* sensory stimuli to elicit *different*, context-specific behavioral strategies. This study uncovers a conserved configuration of electrical synapses, which enables this differential processing of sensory information to deploy context-specific behavioral strategies.

Highlights

- Electrical synapses are required to deploy context-specific behavioral strategies
- Electrical synapses dampen responses to sensory inputs *in vivo* in specific neuron pairs
- Dampened responses suppress context-irrelevant behaviors
- This synaptic configuration enables differential processing of sensory information



Article

Configuration of electrical synapses filters sensory information to drive behavioral choices

Agustín Almoril-Porras,^{1,6} Ana C. Calvo,^{1,6} Longgang Niu,² Jonathan Beagan,¹ Malcom Díaz García,¹ Josh D. Hawk,¹ Ahmad Aljobeh,¹ Elias M. Wisdom,¹ Ivy Ren,¹ Zhao-Wen Wang,² and Daniel A. Colón-Ramos^{1,3,4,5,7,*}

¹Department of Neuroscience and Department of Cell Biology, Yale University School of Medicine, New Haven, CT 06536, USA

²Department of Neuroscience, University of Connecticut Health Center, Farmington, CT 06030, USA

³Wu Tsai Institute, Yale University, New Haven, CT 06510, USA

⁴Marine Biological Laboratory, Woods Hole, MA 02543, USA

⁵Instituto de Neurobiología, Recinto de Ciencias Médicas, Universidad de Puerto Rico, San Juan 00901, Puerto Rico

⁶These authors contributed equally

⁷Lead contact

*Correspondence: daniel.colon-ramos@yale.edu

<https://doi.org/10.1016/j.cell.2024.11.037>

SUMMARY

Synaptic configurations underpin how the nervous system processes sensory information to produce a behavioral response. This is best understood for chemical synapses, and we know far less about how electrical synaptic configurations modulate sensory information processing and context-specific behaviors. We discovered that innexin 1 (INX-1), a gap junction protein that forms electrical synapses, is required to deploy context-specific behavioral strategies underlying thermotaxis behavior in *C. elegans*. Within this well-defined circuit, INX-1 couples two bilaterally symmetric interneurons to integrate sensory information during migratory behavior across temperature gradients. In *inx-1* mutants, uncoupled interneurons display increased excitability and responses to subthreshold sensory stimuli due to increased membrane resistance and reduced membrane capacitance, resulting in abnormal responses that extend run durations and trap the animals in context-irrelevant tracking of isotherms. Thus, a conserved configuration of electrical synapses enables differential processing of sensory information to deploy context-specific behavioral strategies.

INTRODUCTION

Behavioral outputs rely on sensory information. Sensory information can be differentially processed based on the configurations of synapses in the circuit, enabling *similar* sensory stimuli to elicit *different* behavioral strategies in context-dependent manners.^{1–15} This action selection^{16–18} enables animals to avoid deploying incompatible locomotory strategies in response to similar sensory stimuli at behavioral choice points. While the importance of action selection in behavioral choice strategies is well recognized,^{16–18} the synaptic configurations that support action selection are not well understood.

Dissecting action selection mechanisms at a circuit level requires (1) deriving predictable choice points for a given behavioral paradigm, (2) knowing the circuit substrates underlying the behavioral choice points, and (3) understanding sensory input processing and locomotory strategy selection at the behavioral choice points. *C. elegans* thermotaxis behavior¹⁹ provides a tractable model to interrogate the circuitry and synaptic bases of action selection. *C. elegans* does not have an innate preferred temperature and instead learns to prefer the temperature at which it was cultivated in the presence of food (called “cultivation temperature,” or T_c).¹⁹ When in a temperature

gradient, animals perform two behavioral strategies to reach and stay within learned T_c : migrating across the gradient to arrive at T_c (gradient migration) and tracking the isotherms upon encountering T_c (isothermal tracking) (Figure 1; Hedgecock and Russel¹⁹). Isothermal tracking occurs within $\pm 2^\circ\text{C}$ from T_c ,²² and wild-type animals placed in a temperature gradient away from this T_c range will first perform gradient migration, and they will then change their behavioral strategy to isothermal-oriented runs in part via the suppression of turns upon encountering the T_c range (Figures 1A and 1E; Luo et al.²²).

Because the action selection switch between gradient migration and isothermal tracking occurs within the temperature window at which the animal was cultivated (T_c range), thermotaxis behavior provides an assay in which the behavioral choice point is both predictable and quantifiable. Importantly, the specific neurons that underlie thermotaxis behavior have been identified via neuronal ablation and behavioral genetic studies (Figure S1A; Ikeda et al.,¹¹ Mori and Ohshima,²³ Hobert et al.,²⁴ Saterlee et al.,²⁵ Chung et al.,²⁶ Clark et al.,²⁷ Biron et al.,²⁸ Kuhara et al.,²⁹ Beverly et al.,³⁰ and Matsuyama and Mori³¹) and their connectivity is known.³² Briefly, temperature preference depends on a pair of thermosensory neurons called AFDs, which have specialized molecular pathways that allow them to respond



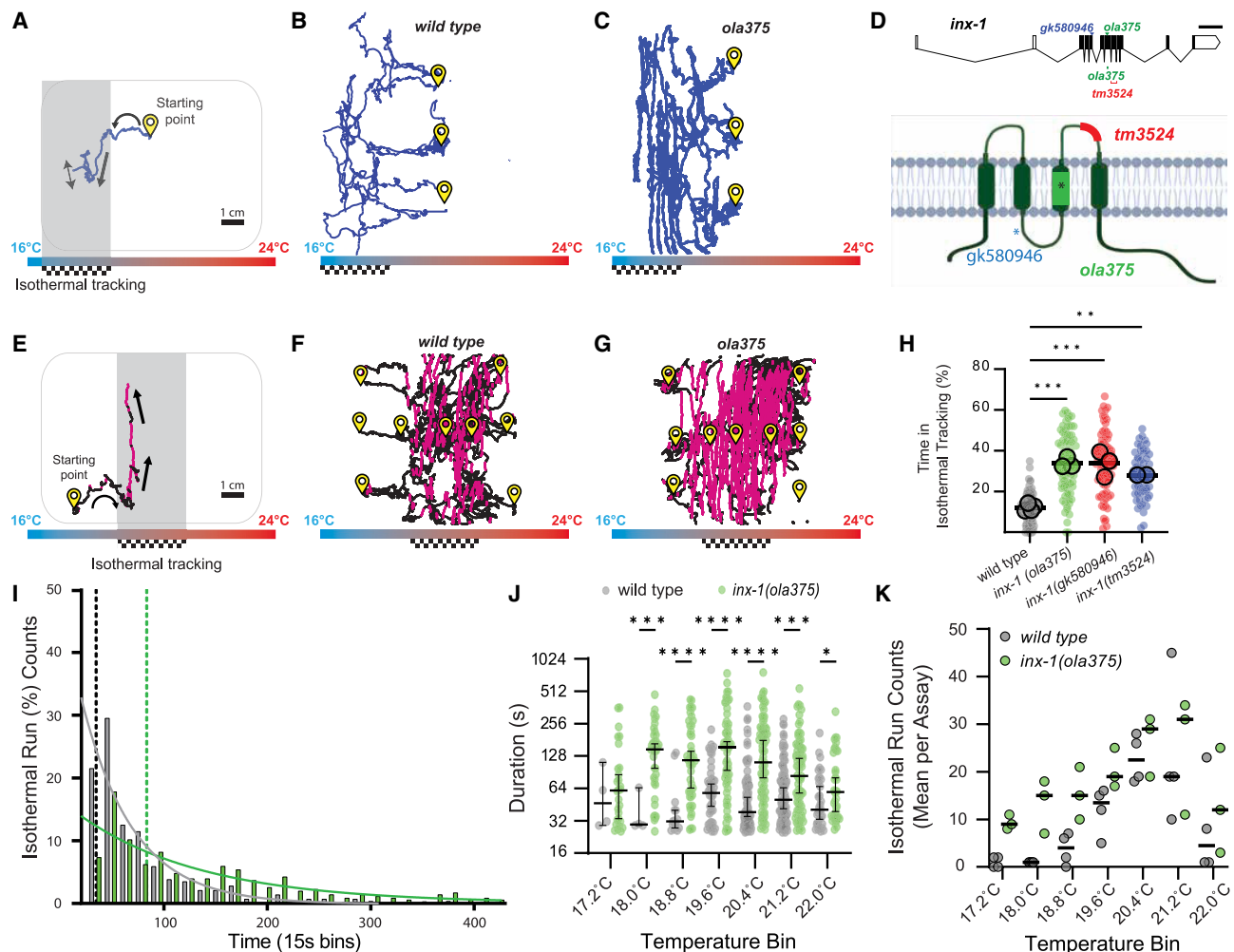


Figure 1. *inx-1* mutants track isotherms at context-irrelevant temperatures

(A) Track of a *C. elegans*, trained at 15°C, performing thermotaxis behavior. *C. elegans* perform two behavioral strategies during thermotaxis: gradient migration toward their preferred temperature and isothermal tracking at their preferred temperature. In the schematic, the preferred temperature region where animals are known to perform isothermal tracking is shaded and highlighted with a checkered goal pattern (bottom). Arrows denote direction of travel. Schematic of circuitry controlling thermotaxis behavior in Figure S1A.

(B) Representative image of wild-type worm tracks for animals trained at 15°C (checkered goal pattern). Animals start points denoted with yellow symbol (middle of gradient). Quantification of time in isothermal tracking and time to reach cultivation temperature in Figures S1B and S1C.

(C) As (B), but for ola375 mutant worms isolated from a forward-genetic screen.

(D) Molecular lesions present in *inx-1* alleles, and their effects on the *inx-1* gene and protein (topology based on Skerrett and Williams²⁰ and Sánchez et al.²¹). The schematic uses *inx-1a.1* isoform. Single-nucleotide polymorphisms include A>G at position X:6,948,431 for *inx-1(ola375)* X and C>T at position X:6,949,062 for *inx-1(gk580946)* X. Insertion/deletions include a 16-bp deletion at position X:6,948,406..6,948,421 for *inx-1(ola375)* X and 238-bp deletion at position X:6,948,032..6,948,269 for *inx-1(tm3524)* X. Introduction of an early STOP codon in W127Opal for *inx-1(gk580946)* X and Y221Opal for *inx-1(ola375)* X. Additional information on genetic lesion corresponding to ola375 allele in Figure S1F. Complementation test in Figures S1G–S1I.

(E) As in (A), but animal is placed on the left-hand side of the gradient and trained at 20°C (checkered goal pattern).

(F) Representative image of wild-type worm tracks for animals trained at 20°C (checkered goal pattern). Animals start points denoted with yellow symbol. Animals were placed in an H-shape configuration in the gradient, as explained in STAR Methods, to better capture gradient migration from multiple directions and isothermal movement in the middle of the gradient. Periods of isothermal tracking automatically recognized (via a quantitative algorithm) are highlighted in red.

(G) As (F), but for ola375 mutant worms.

(H) Percentage of total time animals spent tracking isotherms (per worm track, which includes in the denominator the time spent performing gradient migration) for wild type, ola375 mutants, and two independent *inx-1*-mutant alleles (*inx-1(tm3524)* X and *inx-1(gk580946)* X). Individual track values are presented by semi-transparent single-colored dots, while assay means are represented by bigger-size, slightly transparent circles with a black border. Dark bands represent average of all assays. Colors denote genotypes. ** denotes $p < 0.005$ and *** denotes $p < 0.0005$ by Tukey's multiple comparisons test after obtaining significance ($p < 0.0001$) in a nested one-way ANOVA test. Quantifications of locomotory strategies (omega turns and reversals) across genotypes in Figures S1D and S1E.

(legend continued on next page)

to increases and decreases of temperature as small as $\pm 0.01^\circ\text{C}$.^{22,33,34} Increases in temperature cause depolarization in AFD and activation of its only known chemical postsynaptic partners: a pair of interneurons called AIYs that can initiate and sustain forward-moving runs in multiple behavioral contexts.^{35–40} The main chemical postsynaptic partners to AIYs include bilateral pairs of the interneurons RIAs, RIBs, and AIZs. AIYs also form electrical synapses with bilateral pairs of motor neurons RIMs (White et al.³²; Figure S1A). Laser-ablation studies of neurons in this circuit produces defects in both isothermal tracking and gradient migration,^{11,23–27,41,42} indicating shared circuitry between the two strategies. How synaptic configurations in this circuit influence the processing of thermosensory information to deploy context-specific behavioral strategies is not known.

RESULTS

Mutant allele *ola375* displays abnormal persistence in isotherm-oriented runs

To uncover circuits that underpin action selection mechanisms, we performed behavioral genetic experiments in *C. elegans*. We used traditional thermotaxis assays⁴² as well as an adapted thermotaxis assay designed to enrich for the quantification of isothermal tracking and gradient migration in a population of isogenic animals (Figures 1A, 1B, 1E, and 1F). Individual animals were placed in specific regions of a temperature gradient with respect to their preferred temperature goal (16°C for Figures 1A–1C; 20°C for Figures 1E–1G), and the locomotory trajectories were recorded, segmented, and quantified while they performed gradient migration and isothermal tracking (Figures 1 and S1). Consistent with previous reports,²² wild-type *C. elegans* spent about $\sim 12\%$ of their total time on the assaying arena performing isothermal tracking when within $\pm 2^\circ\text{C}$ of their preferred temperature, with each isothermal run lasting an average of 65 s (Figures 1B, 1F, 1H, and S1B). Distribution of the durations of isothermal track events followed an exponential decay with a time constant of 49.6 s and a half-life of 34.4 s (Figure 1I; Luo et al.²²).

To identify molecules that underlie behavioral choice, we performed an unbiased forward-genetic screen for animals that outperformed wild-type animals in isothermal tracking, irrespective of their preferred temperature, and isolated allele *ola375* (Figures 1C, 1G, 1H, S1B, and S1C). The genetic lesion in *ola375* animals does not affect their temperature preference (as assayed by their capacity to migrate toward their learned cultivation temperature) but displayed defects in abnormally deploying isothermal tracking at temperatures in which the animal would normally be performing gradient migration (Figures 1A–1C, 1E–1G, S1B, and S1C). *ola375*-mutant animals spent $\sim 34\%$ of their time

tracking isotherms, almost three times that of their wild-type counterparts (Figures 1H and S1B). Moreover, the average run duration of the isothermal track for *ola375*-mutant animals was 140.5 s, more than doubling the wild-type average. The distribution of their isothermal run durations still followed an exponential decay (Figure 1I), but the decay rate was two times slower than that of the wild type, with a time constant of 120.1 s and a half-life of 83.2 s. The distributions of run durations for isotherm-oriented runs were consistently higher across temperature gradients in *ola375*-mutant animals compared with wild-type animals (Figure 1J), with the difference being larger near T_c . The number of isotherm-oriented runs initiated was influenced by the distance from their preferred temperature in both the wild type and the *ola375* mutants (Figure 1K). A previous study reported that the wild type performing isothermal tracking “strongly suppresses the occurrence of abrupt reorientation maneuvers,” displaying a 1.25% likelihood of terminating a run by reorientation, in contrast to the 5% likelihood of termination seen during gradient migration.²² Similarly, we observed that wild-type animals performing isotherms displayed 1.65% likelihood of terminating a run. In contrast, *ola375* animals displayed 0.7% likelihood of terminating a run, less than half of that seen in wild-type animals performing isotherms. *ola375* animals also displayed fewer omega turns, as compared with wild-type animals (Figures S1D and S1E). Together, our data indicate that *ola375* animals spent significantly more time than wild-type animals in isotherm-oriented runs.

The *ola375* allele carries a mutation in *inx-1*, encoding a gap junction protein that forms electrical synapses

Genetic characterization of the *ola375* allele revealed it behaved as a recessive single locus lesion. To identify the genetic lesion resulting in the behavioral defects of *ola375* animals, we performed positional mapping and whole-genome sequencing.^{43–46} These strategies revealed a missense mutation and a small insertion-deletion, resulting in an early STOP codon in the fifth coding exon of the gene for innexin 1 (INX-1) (Figures 1D and S1F). Three additional lines of evidence support that *ola375* is a recessive loss-of-function allele of *inx-1*. First, if *ola375* corresponds to *inx-1*, we would expect other alleles of *inx-1* to display similar defects in thermotaxis behaviors. We examined two available alleles (*inx-1(tm3524)* and *inx-1(gk580946)* alleles) and observed that they phenocopied the *ola375* allele in the behavioral defects during thermotaxis (Figure 1E). Second, if *ola375* corresponds to *inx-1*, we would expect a transheterozygote consisting of the *ola375* allele and *inx-1(tm3524)* to display behavioral defects during thermotaxis (in other words, we could expect *inx-1(tm3524)* to fail to complement the *ola375* allele). Consistent with this,

(I) Histogram of the durations of wild-type ($n = 288$) and *inx-1(ola375)X* ($n = 354$) isothermal runs. Solid lines denote best fit for one phase decay curves. Half-lives of the best fit for one phase decay curves are 34.4 s for wild-type animals and 83.2 s for *inx-1(ola375)X* animals, denoted by the two vertical dotted lines. The time constants of the best fit one phase decay curves are $\tau = 49.6$ s for wild-type animals and $\tau = 120.1$ s for *inx-1(ola375)X* animals.

(J) Semi-logarithmic (y axis in \log_2) bee-swarm plot of isotherm-oriented run durations for wild type and *inx-1(ola375)X*, per 0.5°C temperature bin. Values are shown as median \pm 95% CI. * denotes $p < 0.05$, ** denotes $p < 0.001$, *** denotes $p < 0.0001$ by multiple Mann-Whitney tests with a false discovery rate of 1% (using the Benjamini, Krieger, and Yekutieli method).

(K) Assay means of number of isotherm-oriented runs for wild-type and *inx-1(ola375)X* animals, per 0.5°C temperature bin.

See also Figure S1.

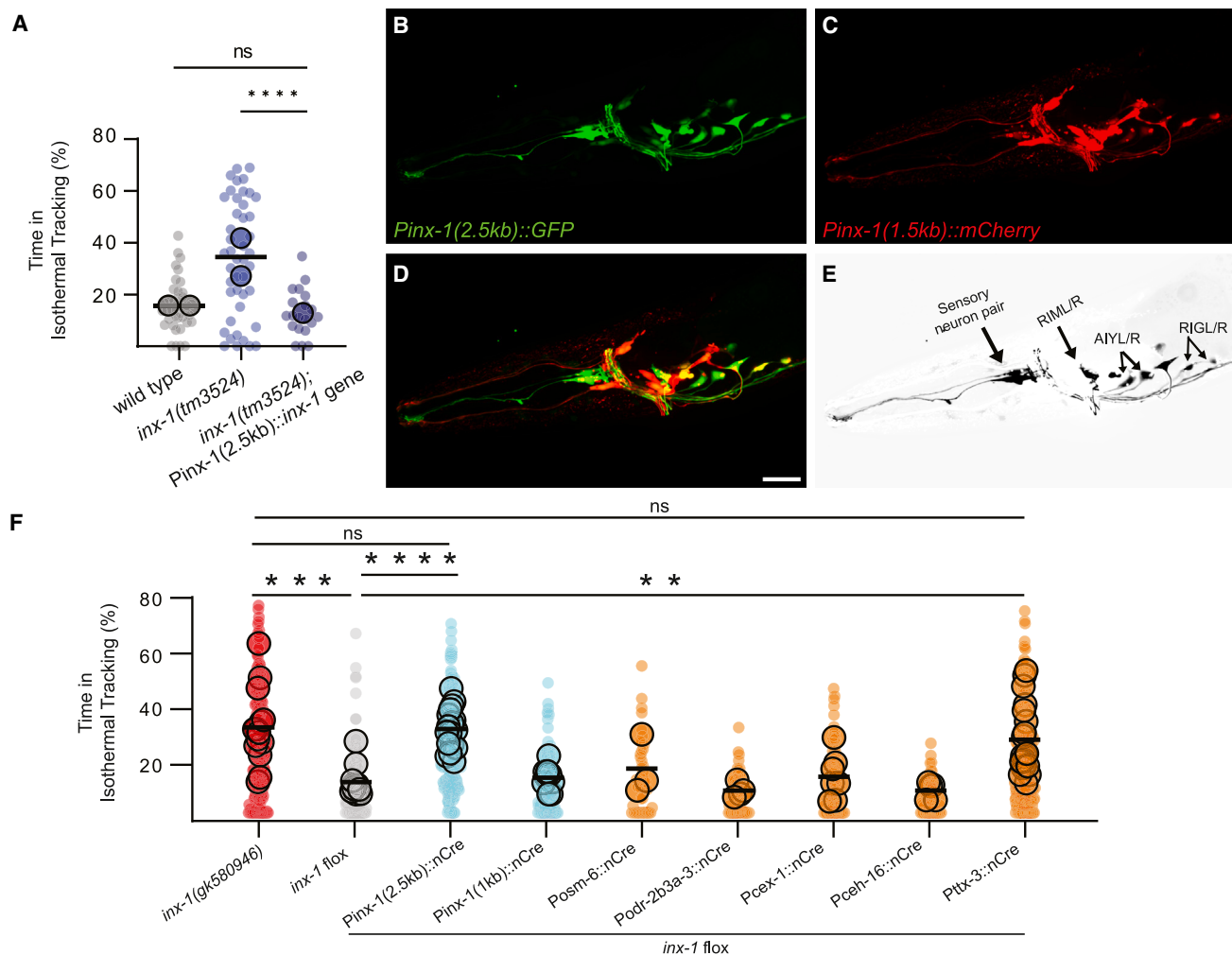


Figure 2. INX-1 is required in AIY interneurons to suppress context-irrelevant isothermal tracking

(A) Percentage of time animals spend tracking isotherms, per worm track, for wild type, *inx-1(tm3524)X* mutants, and *inx-1(tm3524)X; olaEx2136* (*inx-1* rescue). *** denotes $p < 0.0001$ by Dunnett's T3 multiple comparisons test after obtaining significance in both Brown-Forsythe ($p < 0.0001$) and Welch's ($p < 0.0001$) ANOVA tests on the individual tracks. Individual track values are presented by semi-transparent single-colored dots, while assay means are represented with bigger-size, slightly transparent dots with black borders. Dark bands represent average of all assays. Colors denote genotypes.

(B) Fluorescent micrograph of the head of an animal expressing GFP under the control of the rescuing 2.5 kb *inx-1* promoter.

(C) Fluorescent micrograph of the head of an animal expressing mCherry under the control of the 1.5 kb *inx-1* promoter.

(D) Composite of (B) and (C). Scale bar is 50 μ m and applied to (A)–(C) and (E).

(E) Neuronal pairs present under the 2.5-kb *inx-1* promoter but not the 1.5-kb *inx-1* promoter (for strategy, see Figure S2A).

(F) Percentage of time animals spend tracking isotherms, per worm track, for indicated genotypes. *inx-1(ola278)* (in the graph called "inx-1 flox") is an engineered *inx-1* floxed allele for conditional knockdowns using Cre recombinase (see Figure S2B). Cre recombinase was expressed in the *inx-1* floxed allele under the indicated promoters. *Posm-6* drives expression in most ciliated neurons in *C. elegans*, including AFD.⁴⁷ *Podr2b3a* is a based promoter from *Podr2b*,⁴⁸ which drives expression primarily in AIZ and AIB interneurons. *Pcey-1*, *Pceh-16*, and *Ptx-3G* drive cell-specific expression in RIM, RIG, and AIY, respectively. ** denotes $p < 0.01$, *** denotes $p < 0.001$, **** denotes $p < 0.0001$ by Kruskal-Wallis test. Individual track values are presented by semi-transparent single-colored dots, while assay means are represented by bigger-size, slightly transparent dots with a black border. Dark bands represent average of all assays. See also Figure S2.

we observed that *inx-1(tm3524)* failed to complement *ola375* alleles (Figures S1G–S1I), suggesting that the *tm3524* and *ola375* alleles correspond to genetic lesions within the same gene, *inx-1*. Third, if *ola375* corresponds to *inx-1*, we would expect transgenic expression of wild-type *inx-1* genomic DNA to rescue the thermotaxis behavioral phenotype of *inx-1(tm3524)* mutants, which we observed (Figure 2A).

INX-1 is a member of the innexin family of proteins, which is functionally and topologically related to vertebrate connexins.^{49–54} Connexins can form gap junctions in vertebrates, and innexins do so in invertebrates.^{50,51,55–62} In *C. elegans*, *inx-1* is expressed in neurons and body wall muscles.^{63,64} It contributes to the electrical coupling of body wall muscle cells⁶⁵ and synchrony of neuronal activities during rhythmic behavior.^{66,67}

INX-1 functions in AIY interneurons to suppress context-irrelevant isothermal tracking

Rescue experiments with *inx-1*, using different lengths of the *inx-1* promoter, revealed that expression of wild-type *inx-1* in *inx-1(tm3524)* mutants under the control of a 2.5-kb but not a 1.5-kb promoter sequence (upstream of the *inx-1* translation initiation site) could rescue the mutant behavior (Figures 2 and S2). To identify the neurons where INX-1 acts to regulate the thermotaxis behavior strategies, we expressed GFP under the control of the *Pinx-1(2.5 kb)* promoter fragment (Figure 2B) and mCherry under the *Pinx-1(1.5 kb)* (Figure 2C) fragment, respectively, and used a subtractive strategy to identify the neurons in which *inx-1* is likely required for rescue (Figures 2B–2E and S2A). This strategy identified four pairs of neurons that were detected with the longer (rescuing) but not the shorter *Pinx-1* promoter fragment: AIYs, RIMs, RIGs, and an unidentified amphid neuron. To determine whether only one specific pair of these neurons is required for the *inx-1* function, we generated cell-specific conditional knockout strains by flanking the *inx-1* gene with *loxP* sites (Figure 2B; Dickinson et al.⁶⁸) and expressing Cre⁶⁹ in the candidate neurons by using cell-specific promoters (*Ptx-3G* for AIY, *Pcex-1* for RIM, and *Pceh-16* for RIG). We observed that knockout of *inx-1* in AIYs (but not in other neurons, including RIM and RIGs) recapitulated the aberrant action selection phenotype observed in *inx-1* mutants (Figure 2F). Consistent with this, AIY-specific expression of wild-type *inx-1* abrogated the isothermal tracking phenotype of the *inx-1(tm3524)* mutants. The expression of wild-type *inx-1* in AIY also caused an abnormal gradient migration phenotype, presumably from *inx-1* overexpression (Figures 2C–2F; Hawk et al.⁷⁰).

INX-1 electrical synapses between AIYs serve to dampen excitatory inputs

The AIY neuron class consists of two bilaterally symmetric interneurons that are required for proper thermal gradient migration and isothermal tracking.^{11,22–24,31,42,71,72} They are the only known chemical postsynaptic partners to the bilateral pair of thermosensory neurons, AFDs (White et al.³² and Witvliet et al.⁷³; Figure S1A). AIY also forms electrical synapses onto interneuron RIM, and this electrical synapse is necessary for persistent neural activity and sustained behavioral patterns.⁷⁴ Electron microscopy studies of the *C. elegans* connectome have also predicted an electrical synapse between the two AIYs at their synaptic regions,³² but the physiological function and molecular composition of these structures remain unknown. Since cell-specific knockout of *inx-1* in RIM did not restore the *inx-1*-mutant phenotypes (Figure 2F), we focused our analyses on AIY and investigated how loss of *inx-1* affected AIY responses, whether the AIY pair is electrically coupled, and whether this coupling relies on INX-1.

To answer these questions, we used transgenic animals expressing the genetically encoded calcium indicator GCaMP6 in AIY and assessed the effect of depolarizing one AIY (referred to as the voltage-clamped AIY [AIY_c]) on the calcium dynamics of both AIY_c and the unclamped AIY (AIY_{uc}). We depolarized from -60 to +40 mV for 1, 3, or 20 s and quantified the calcium signal within a region known as zone 2 (Figure 3A),⁷⁵ where the two AIYs have been shown to respond to thermal stimuli^{27,70}

and have exhibited, by EM, morphologically defined gap junctions between them.³² In response to the voltage step, calcium signals increased in both AIYs of wild-type animals (Figures 3B, 3C, and S3). In contrast, in *inx-1(gk580946)*-mutant animals, only AIY_c responded, with the difference in the ratio of AIY_{uc}/AIY_c calcium intensity being statistically significant for the voltage steps of 3- and 20-s durations (Figures 3B, 3C, S3B, and S3D). The calcium signal ratio of the AIY pair (unclamped over clamped) during the depolarizing voltage step (+40 mV) was 0.85 ± 0.06 in the wild type and 0.19 ± 0.05 in the *inx-1* mutants (Figure 3D), indicating that INX-1 is required for the activation of AIY_{uc}. The calcium signal of AIY_{uc} remained quiet prior to the voltage step (while AIY_c was held at -60 mV) in all wild-type animals, but it fluctuated in four of six *inx-1(gk580946)*-mutant animals (Figure 3A). These results indicate that the hyperpolarizing voltage (-60 mV) could effectively silence the calcium activity of both AIYs in wild-type animals, but only in AIY_c in *inx-1* mutants, further suggesting that the two AIYs are electrically coupled by INX-1 gap junctions.

Considering that INX-1 forms electrical synapses between the two AIYs, we explored how the absence of these electrical synapses might enhance isothermal tracking. To address this question, we began by measuring the membrane resistance (R_m) and membrane capacitance (C_m) of AIY. In wild-type animals, the observed responses of AIY to current injections were consistent with those previously reported (membrane voltage responses to positive current injections were smaller than those to negative current injections).⁷⁶ We then examined *inx-1* mutants and observed a significant increase in R_m and a substantial reduction in C_m in *inx-1(tm3524)* mutants, compared with the wild type (Figures 4A–4C). As R_m relies on membrane conductance, and C_m is directly proportional to the cell membrane area, our results support the idea that the measured R_m and C_m values reflect the contributions of both AIYs in the wild type but only one AIY in the *inx-1* mutant. We predicted that the increased R_m and reduced C_m would make AIY neurons hyperresponsive to applied stimuli. Indeed, when we injected current into one AIY, it induced greater changes in membrane voltage of that same AIY in the *inx-1* mutant, as compared with the wild type (Figure 4D). Collectively, these findings suggest that gap junctions may serve to dampen AIY responses to sensory inputs by shunting excitatory currents. This configuration is reminiscent to that of electrical synapses in amacrine cells of the retina and midbrain mesencephalic trigeminal nucleus neurons (MesV), in which electrical synapses dampen responses, resulting in reduced noise during sensory processing.^{78–81} Together, our findings suggest that disrupting coupling between the bilaterally symmetric AIYs enhances individual AIY responses, making them hyperresponsive to sensory stimuli.

AIY sensitization in *inx-1*-mutant animals increases response frequency to small temperature changes

AIY activity is known to regulate animal locomotion by suppressing turns to induce and sustain bouts of forward movement, or “runs”^{35–40,82}. During isothermal tracking, animals strongly suppress reorientation maneuvers to persist in runs.²² Since this phenotype is abnormally enhanced in *inx-1* mutants (Figures 1 and S1), we hypothesized that in *inx-1*-mutant animals, the

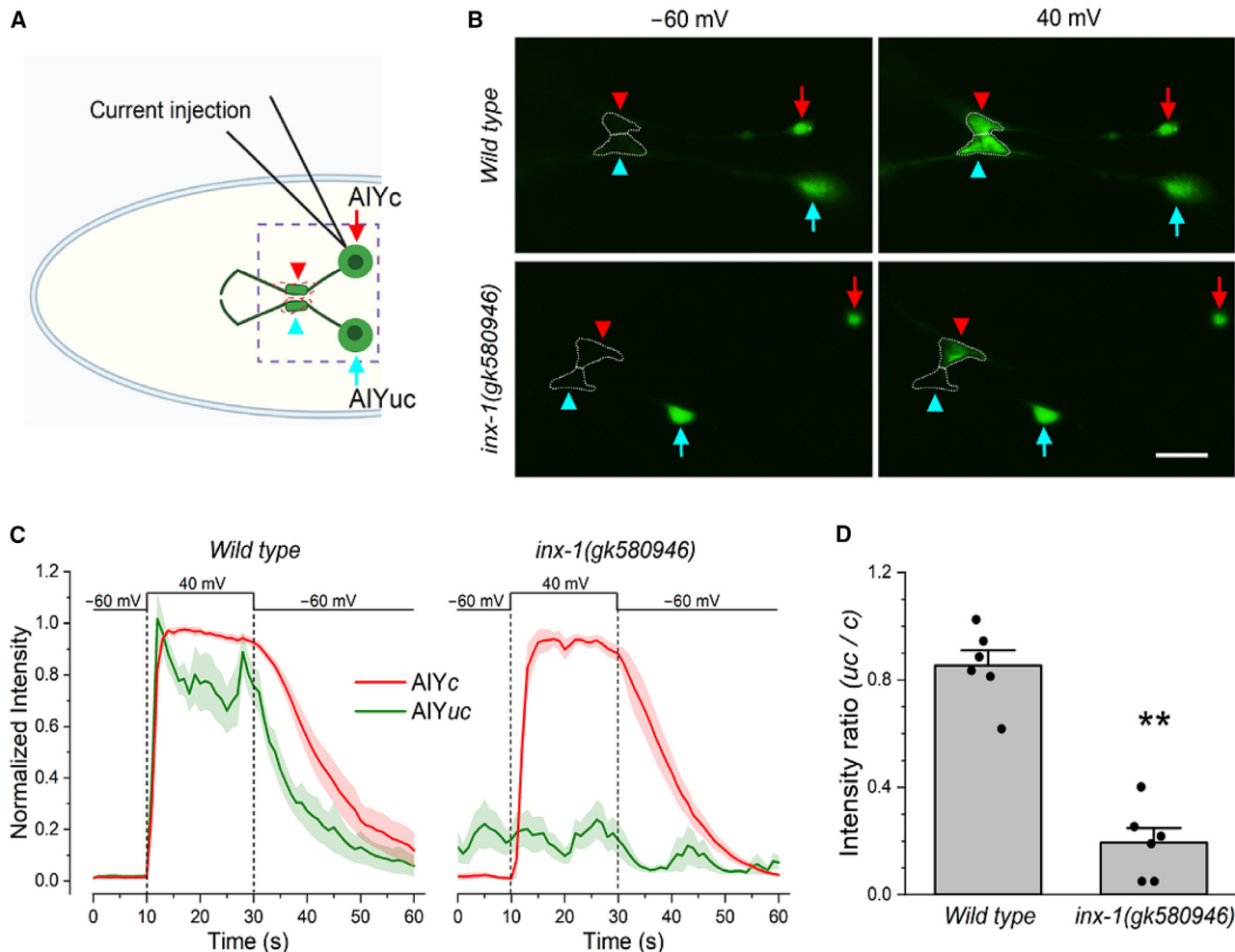


Figure 3. The bilateral pair of AIY interneurons are electrically coupled by INX-1 gap junctions

(A) Schematic of the *C. elegans* head with the two AIYs labeled AIY_c (voltage clamped) and AIY_{uc} (unclamped), respectively. The arrowheads and arrows mark the synaptic regions and cell bodies of the AIYs, respectively. The dashed box corresponds to the imaging region in (B).

(B) Sample images of GCaMP6 fluorescence in the two AIYs of wild-type and *inx-1(gk580946)* animals before (holding voltage -60 mV) and during the 40 -mV voltage step. The arrowheads and arrows label the same regions of AIYs as in (A).

(C) Group average of GCaMP6 signal over time in AIY_c and AIY_{uc} of wild-type and *inx-1(gk580946)* animals. The results of individual animals that gave rise to the group average are displayed in Figure S3A. Traces are shown as mean \pm SE.

(D) Comparison of GCaMP6 signal ratio ($\text{AIY}_{uc}/\text{AIY}_c$) between wild type and the *inx-1(gk580946)* mutant ($n = 6$ in both groups). The average GCaMP6 signal during the last 15 s of the 40 -mV voltage step was used for the comparison. Values are shown as mean \pm SE. The asterisks (**) indicate a statistically significant difference compared with wild type ($p < 0.01$, unpaired t test). For results showing varying depolarizing periods, see Figure S3.

See also Figure S3.

uncoupled and hyperresponsive AIY interneurons might display an increased probabilistic response rate to sensory stimuli, including to small-scale changes in temperatures (like those experienced by the animals tracking isotherms). The hyperresponsiveness in AIYs might therefore result in suppressed turns and sustained runs during the small temperature fluctuations that animals experience during isotherms.

To examine this hypothesis, we first determined the temperature experiences of animals performing isothermal tracking versus gradient migration by modeling (1) head bends, by fitting a sinusoidal function to positional measurements of the nose of an animal as it freely navigates a temperature gradient (Figures

5A and S4A), and (2) bouts of forward movement, by recording the speed of animals as they move directly up a temperature gradient and fitting the data with a lognormal distribution (Figures 5A, 5B, and S4B). Our calculations indicate that animals performing isothermal tracking under our experimental conditions experience oscillations, with each head bend, deviating $\pm 0.011^\circ\text{C}$ from the absolute temperature being tracked. This result is consistent with the known AFD temperature limit of 0.01°C ^{22,33,34} and consistent with previous estimates for experienced temperatures during isothermal tracking.²² Therefore, an animal performing a perfect isotherm in our experimental conditions will experience a net temperature change of 0.022°C for

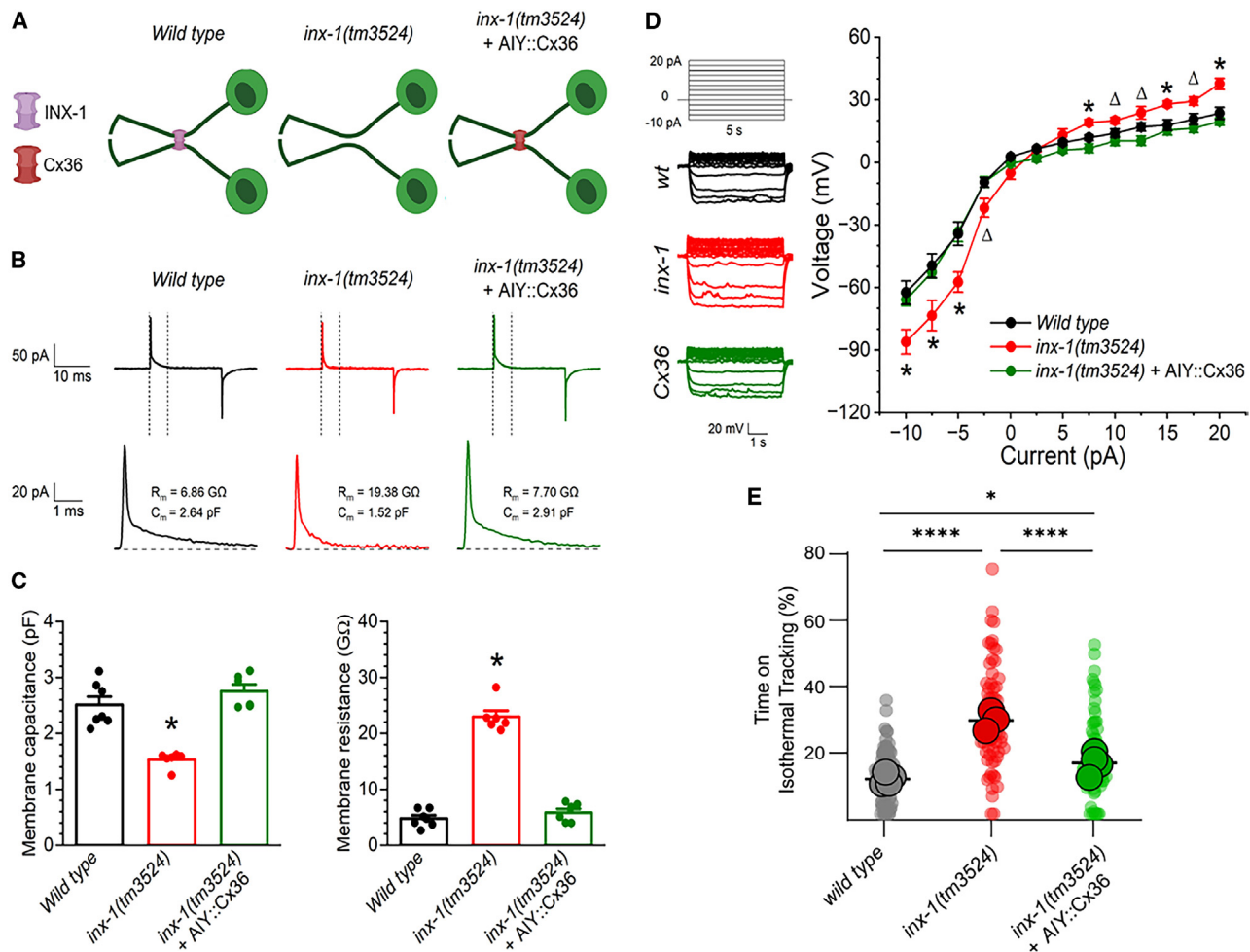


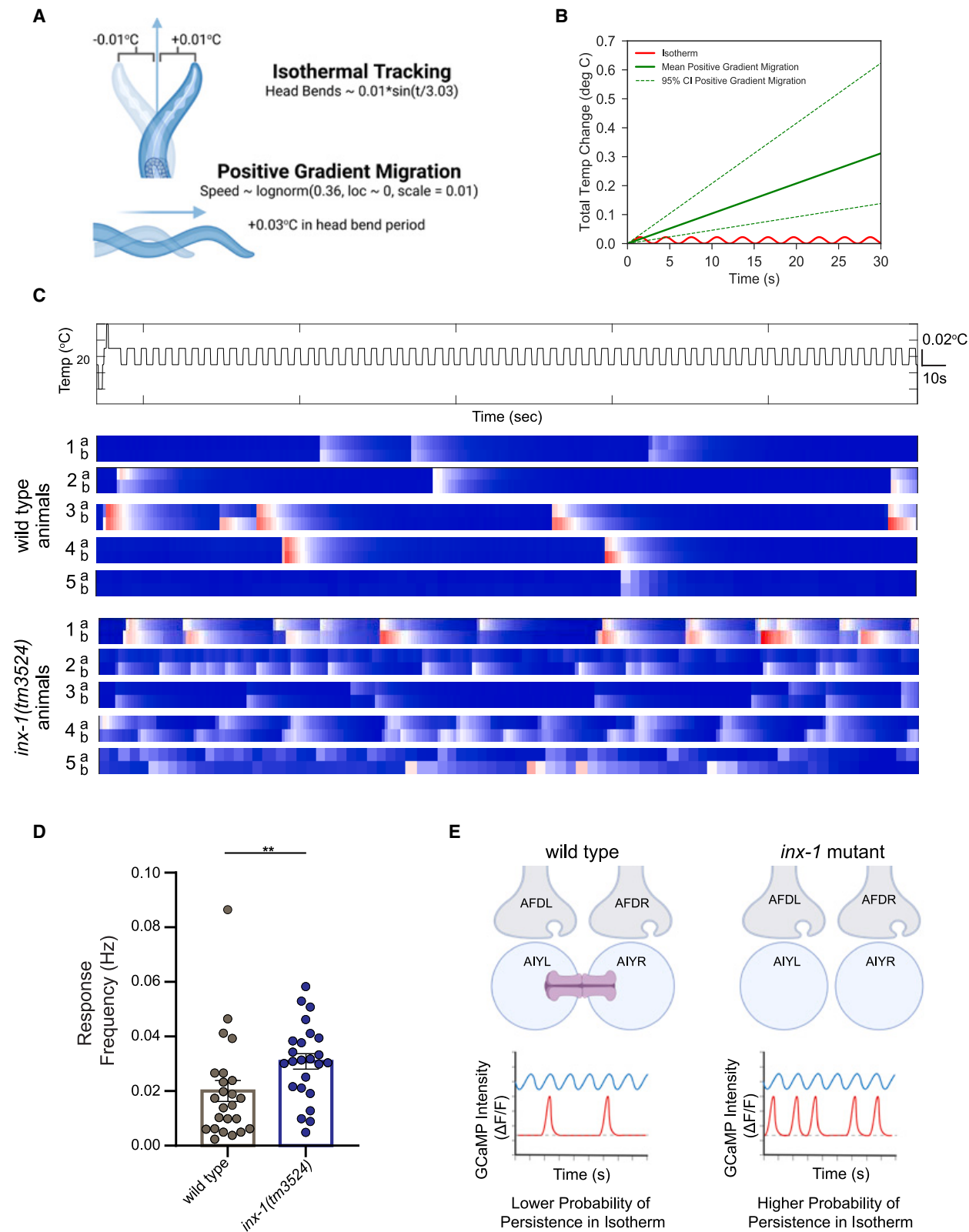
Figure 4. INX-1 electrical synapses regulate AIY excitability through effects on membrane capacitance and membrane resistance

(A) Schematic of the bilateral AIY interneuron cell bodies and neurites with INX-1 electrical synapses in wild type, no electrical synapses in *inx-1(tm3524)*, and connexin 36 (Cx36) electrical synapses in *inx-1(tm3524)* expressing Cx36 in AIYs (using *Ptx-3G*, a promoter fragment known to express cell specifically in AIY⁷⁷). (B) Top: representative current traces induced by a membrane test protocol (a voltage step of +20 mV for 20 ms from a holding voltage of -60 mV). Bottom: the regions marked by the vertical dotted lines in the top traces are shown at a faster timescale. The displayed membrane resistance (R_m) and membrane capacitance (C_m) values were from running the membrane test protocol. (C) Comparison of membrane capacitance and membrane resistance among wild type, *inx-1(tm3524)*, and *inx-1(tm3524)*-expressing Cx36 in AIYs. Values are shown as mean \pm SE. (D) Voltage versus current relationships of wild type, *inx-1(tm3524)*, and *inx-1(tm3524)*-expressing Cx36 in AIYs. Values are shown as mean \pm SE. (E) Expression of Cx36 in AIYs of *inx-1(tm3524)* rescued the mutant isothermal tracking phenotype. Each dot represents a single track, and each circle represents one assay. Dark bar represents the average of all assays. Results of the transgenic group were obtained for three independent lines. In (C) and (D), the sample size (n) was 7 in wild type and 6 in each of the remaining two groups. The single and double asterisks (*) and (***) indicate statistically significant differences at $p < 0.05$ and $p < 0.01$, respectively (one-way ANOVA with Tukey's post hoc test). In (E), the single and quadruple asterisks (*) and (****) denote statistically significant differences at $p < 0.05$ and $p < 0.0001$, respectively (Dunn's multiple comparisons test following a Kruskal-Wallis test).

each completed head bend, but over time, as it tracks the isotherm, the integrated net change in temperature would be zero. In contrast, during the same head-bend period of 3 s, animals moving up the gradient (at median speed) experience an increase in temperature of 0.03°C (Figure 5B), and in a period of 10 s, they will experience temperature changes that are an order of magnitude larger than the largest temperature change experienced by an animal performing isothermal tracking (Figure 5B). Based on our model and the known probabilistic nature of AIY responses upon AFD activation (during increases of temperat-

ure),³⁴ we hypothesized that AIY activation might be significantly different in *inx-1*-mutant animals, compared with wild-type animals, particularly under conditions of small-scale temperature changes such as those seen during isothermal tracking.

To test this hypothesis, we imaged calcium dynamics of both AIYs in immobilized wild-type and *inx-1*-mutant animals after conditioning them at 20°C for several hours and presenting them with oscillating temperature stimuli (every 4.1 s) centered around 20°C (with an amplitude of $\pm 0.01^\circ\text{C}$) (Figure 5C). In the wild type, calcium transients occurred at a low rate of 0.020 Hz



(legend on next page)

(one response every ~50 s). These responses in the wild type were often concurrent in the two AIYs, with a Pearson's correlation coefficient of 0.72 (Figures 5C, 5D, and S4C). In contrast, calcium transients occurred at a significantly higher frequency of 0.031 Hz (or one response every ~32 s) and were more asynchronous (Pearson's correlation coefficient of 0.36 between the two AIYs) in *inx-1(tm3524)*-mutant animals, as compared with the wild type (Figures 5C, 5D, and S4C; Videos S1 and S2). Our findings support a model in which the uncoupled AIYs in *inx-1* mutants respond more frequently than those in wild-type animals to changes in temperature, including small-magnitude temperature changes like those seen during isothermal tracking.

In combination with previous findings that determined that activation of AIY sustains forward movement runs,^{35–40,82} our data support a model in which *inx-1*-mutant animals are “trapped” in long runs in response to subthreshold sensory stimuli, resulting in increased isothermal tracking behavior (Figure 5E). Our model predicts that *inx-1* animals would perform longer runs under all conditions, including those outside of a temperature gradient, as AIY would also become activated by sensory stimuli and lock animals in runs (but not in isotherms, as they would not be in a temperature gradient). To test this, we performed run dispersion assays in an arena without a temperature gradient (in these assays, AIY responses are still expected due to existing presynaptic inputs and sensory stimuli, including those from chemosensory neurons that directly innervate AIY³²). Consistent with our hypothesis, we observed that *inx-1(ola375)* mutants performed significantly longer runs, as compared with wild-type animals (Figure S4D).

Expression of Cx36 just in AIYs suppresses context-irrelevant isothermal tracking in *inx-1* mutants

Innexins can form homotypic or heterotypic gap junctions between neighboring cells.⁸³ Our loss-of-function experiments indicate that INX-1 is necessary, cell specifically, in the AIYs to couple these bilaterally symmetric interneurons. But the INX-1-dependent gap junction could be forming between the two AIYs or onto other cells (such as RIM, which is also electrically coupled to AIY^{32,74}). The question arises, is a gap junction between just the two AIYs sufficient to explain the observed behavioral phenotypes? To address this, we introduced vertebrate connexin 36 (Cx36) specifically into AIYs of *inx-1(tm3524)* animals (by

using the cell-specific promoter fragment, *Ptx-3G*⁷⁷) and examined if reconstituting this heterologous gap junction was sufficient to suppress the electrophysiological and behavioral *inx-1*-mutant phenotypes. Vertebrate connexins do not interact with the endogenous innexins, and introduction of Cx36 cell specifically onto AIY would only couple the bilaterally symmetric AIYs.^{84,85} We observed that expression of Cx36 specifically on AIYs suppressed the significant increase in R_m and the reduction in C_m in *inx-1(tm3424)* mutants, restoring them to wild-type levels (Figures 4A–4D). Moreover, the transgenic animals expressing Cx36 specifically in the AIY interneurons exhibited a significant decrease in the time spent on isothermal tracking, compared with the original *inx-1(tm3524)* mutant (Figure 4E). These results provide further support to the idea that the abnormal thermotaxis behavior of the *inx-1* mutants specifically results from the loss of electrical coupling between the two AIYs.

DISCUSSION

We uncovered a specific configuration of electrical synapses which is necessary *in vivo* for context-dependent action selection. These electrical synapses form between bilaterally symmetric AIY interneurons to decrease R_m and increase C_m , which in turn dampen the effects of subthreshold excitatory synaptic inputs onto AIYs. The bilateral coupling of the AIY interneurons is necessary for animals to “filter” sensory information of subthreshold magnitude and for the animal to suppress isotherms to correctly migrate across the temperature gradients toward its preferred temperature. INX-1 has been previously shown as necessary for the execution of rhythmic behavior regulated by the AVL and DVB neurons. These two neurons are coupled via an INX-1-dependent electrical synapse that synchronizes their presynaptic terminals and inhibits their ectopic activation between rhythmic cycles.⁶⁶ Our findings are consistent with these roles of *inx-1* in inhibiting ectopic responses and extend them to demonstrate that in AIYs this coupling is necessary to inhibit activation in response to subthreshold sensory stimuli. Uncoupled interneurons in the *inx-1* mutants result in hyperresponsive AIYs that trap animals in context-irrelevant isotherms, affecting correct action selection during thermotaxis behavior.

AIY calcium activity is required to initiate and sustain a forward-moving run in multiple behavioral contexts.^{35–40} Our

Figure 5. AIY sensitization in *inx-1*-mutant animals increases response frequency to small temperature changes

- (A) Diagram depicting modeled temperature changes induced by head bends in isothermal run (top) and forward movement directly up temperature gradient (bottom). The calculations used for the model are in Figures S4A and S4B and are consistent with previous studies.²²
- (B) Quantification of total temperature changes evoked by models presented in (A) as a function of run duration.
- (C) Calcium responses of wild type (top) and *inx-1* mutants (bottom) immobilized animals when stimulated by an isotherm ($\pm 0.01^\circ\text{C}$ oscillations around $T_c = 20^\circ\text{C}$ [schematic of stimuli above plots]). Color scale indicates $\Delta F/F$ GCaMP intensity, with red being more intense than blue. For each animal (numbered to the left of the calcium traces), the two bilaterally symmetric AIYs were recorded (indicated as “a” and “b”). See also related Videos S1 and S2 and Figures S4C and S4D.
- (D) Frequency of individual AIY calcium transients in wild-type animals (12 animals, 24 AIYs) and *inx-1(tm3524)* mutants (12 animals, 24 AIYs). Values are shown as mean \pm SE and the asterisks ** denotes $p < 0.01$ by two-tailed Mann-Whitney test.
- (E) Schematic model of AFD to AIY signaling, and resulting behavior, in wild type versus *inx-1* mutants. In wild-type animals, coupled AIYs have lower resistance, which would result in dampened responses to thermosensory stimuli coming from AFD. These dampened responses enable AIYs to integrate larger changes of thermosensory information as animals perform gradient migration. In *inx-1* mutants, uncoupled AIYs are hyperexcitable due to a change in their electrophysiological properties resulting from the uncoupling. This hyperexcitability results in AIYs responding to subthreshold sensory signals. Activation of AIY initiates and sustains a forward-moving run,^{35–40} and their hyperresponsiveness to subthreshold stimuli would result in a higher probability of animals abnormally persisting in isotherms.

See also Figure S4.

findings support a model in which the probability of AIY activation accounts for the behavioral differences observed between the wild type and the *inx-1* mutants. In wild-type animals, AIYs have a low level of activity at the initiation of an isotherm-oriented run far away from their preferred temperature. The absence of activity would result in the probabilistic exit from the isothermal orientation via the execution of a reversal or pirouette,^{22,39} thereby ending the run and reorienting the animal in a different direction. However, hyperresponsive AIYs in *inx-1* mutants would be activated by stimuli that are subthreshold for AIY activation in wild-type animals. The hyperresponsiveness of AIYs in *inx-1* mutants would lead to the persistence of isotherm-oriented runs and for animals to be “trapped” in this behavioral state.

Wild-type animals also track isotherms, but unlike *inx-1* mutants, this behavioral strategy is restricted to a temperature context near ($\pm 2^\circ\text{C}$) of their cultivation temperature (T_c).^{11,19,22} Like *inx-1* mutants, wild-type animals also suppress reorientations and turns to persist in runs during isotherms, but unlike *inx-1* mutants, they do so in the correct context (near T_c).²² We hypothesized that in the wild-type animals near T_c , signal gains in the AFD → AIY synapse lead to activation of AIY in response to smaller temperature derivatives at the preferred cultivation temperature to promote isothermal tracking performance near T_c . The gain of AFD → AIY could be achieved via INX-1, which could serve as a regulatory switch for modulating action selection in wild-type animals. In *C. elegans*, expression of innexins can be plastically regulated in a neuron-type and environment-specific manner.⁶⁴ The open/close states of electrical synapses can also be regulated by other molecules or posttranslational modifications.^{57,60,86–90} We therefore posit that regulation of INX-1 may be a molecular substrate that enables a plastic uncoupling of the AIY pair and that this uncoupling could change sensory processing to ultimately affect action selection.

Specific configurations of electrical synapses can support circuit architectures with unique properties, and the organization of electrical synapses between the two AIYs might be a conserved and important configuration in sensory processing. For example, in vertebrates and invertebrates, a central hub neuron can be electrically coupled to multiple input neurons to form hub-and-spoke circuits. Hub-and-spoke circuits can modulate integration of sensory processing, perception, and behavioral responses.^{91,92} In AIY, coupling of this interneuron to motor neuron RIM via an electrical synapse is important for encoding both temperature and motor-state information.⁷⁴ In this study, we find another configuration of electrical synapses, linking bilaterally symmetric interneurons to alter their electrophysiological responses and sensory processing. Most interneurons in *C. elegans* are bilaterally symmetric and coupled via gap junctions,³² and we speculate that this architecture might represent a circuit motif by which the system modulates neural gain. Consistent with this, in our previous study, we identified an electrical coupling between right and left AVA locomotor interneurons, which equilibrates asymmetric synaptic inputs from inhibitory GABAergic neurons to guide correct behavioral selection in response to mixed threat and reward sensory cues.⁹³ These configurations are reminiscent of the gap junction organization between amacrine cells in the retina. Amacrine cells are coupled

by gap junctions that are critical for coincidence detection by photoreceptors, noise reduction, and sensory processing during light adaptation.^{78–81} In *inx-1* mutants, synchronous excitation between the two AIY pairs is also lost and might also represent a property of the circuit in performing coincidence detection, which could then be important in noise reduction and sensory processing of the temperature gradient, or its integration with other sensory responses. Together, our findings reveal a conserved electrical synapse configuration that might confer circuits the ability to deploy context-dependent plastic responses by dynamically modulating sensory information processing, thereby increasing the versatility of neural circuits during sensory stimuli.

Limitations of the study

In this study, we uncovered a role for INX-1 in AIY in regulating its electrophysiological properties to modulate sensory processing and action selection. While our cell-specific knockouts of INX-1 in AIY show that INX-1 is necessary in AIY for the observed phenotypes, and our expression of Cx36 in AIY of *inx-1* mutants demonstrate that an electrical synapse between the two AIYs is sufficient to reverse the *inx-1* phenotypes, our experiments do not exclude the possible requirement of other innexins that might pair with INX-1 in forming the electrical synapse between the two AIYs.

Our findings provide a molecular foothold to understand how action selection in the thermotaxis behavioral paradigm might happen in wild-type animals, but our study focused on understanding *inx-1* mutants and did not examine its molecular regulation in wild-type animals or the changes wild-type animals undergo when performing isothermal tracking. While we speculate that INX-1 might be a substrate for regulation in wild-type animals, this needs to be empirically tested. We also emphasize that there could be other ways beyond the regulation of INX-1 electrical synapses, which could affect sensory processing in the AFD → AIY synapse and which would be consistent with our results, including presynaptic facilitation or increased responses of AFD near the cultivation temperature range.

Our findings demonstrate a role for INX-1 in modulating R_m and C_m in AIY, as well as its responses to sensory stimuli. While it is known that activation of AIYs results in suppression of turns and forward movement,³⁸ the link between increased AIY activity observed in *inx-1* mutants and forward movement is based on the untested assumption that activation of a single AIY interneuron is sufficient to result in forward movement. INX-1 couples the two AIYs, and coupling of the AIYs might contribute to coincidence detection. Coincidence detection could occur from signals from the two AFD sensory neurons or from other sensory neurons known to form presynaptic specializations onto AIYs (including chemosensory neurons AWA, AWC, and ASE).³² *C. elegans* crawls on its side (flexing in a dorsoventral direction), and in our assays (performed in flat plates), the bilaterally symmetric AFDs are sampling the same thermal space of the gradient. However, *C. elegans* evolved to navigate a 3D environment, and in that context, the two AFD neurons might sample different thermal spaces in ways in which coincidence detection would be important for tracking 3D isotherms. Future behavioral studies examining responses in freely moving animals,

preferably in 3D environments, will be necessary for understanding the role of coincidence detection proceeding from AFD or other sensory neurons in these responses.

Despite these limitations of the study, our data support the following mode: electrical coupling of the AIY interneurons via INX-1 electrical synapses is necessary for animals to “ignore” isotherms in contexts in which they perform gradient migration. In *inx-1* mutants, AIY interneurons are uncoupled, displaying increased excitability due to increased R_m and reduced C_m . This causes AIY to respond to the subthreshold sensory stimuli like those encountered during isotherms. Because stimulation of AIY suppresses turns and promotes runs, this excitability would cause extended run durations and “trap” animals in isotherms, including isothermal runs in the incorrect contexts. The observed configuration of electrical synapses might be a conserved circuit configuration that enables differential processing of sensory information to deploy context-specific behavioral strategies.

RESOURCE AVAILABILITY

Lead contact

Further information and requests for resources and reagents should be directed to and will be fulfilled by the lead contact, Daniel Colón-Ramos (daniel.colon-ramos@yale.edu).

Materials availability

Plasmids and strains generated in this study are available upon request to the lead contact.

Data and code availability

- All behavior raw data can be found as of the date of publication, on GitHub: <https://doi.org/10.5281/zenodo.14170612>. Calcium-imaging acquisitions are available upon request to the lead contact due to the large file sizes.
- All original codes can be found on the publicly available GitHub: <https://doi.org/10.5281/zenodo.14170612>.
- Any additional information needed to reanalyze the data reported here can be obtained from the lead contact.

ACKNOWLEDGMENTS

We thank the members of the Colón-Ramos lab and the scientific community for their thoughtful comments on the project. We thank Netta Cohen (University of Leeds), Alberto Pereda (Albert Einstein College of Medicine), and Peri Kurshan (Albert Einstein College of Medicine) for constructive feedback and helpful discussions on the project. We thank the *Caenorhabditis* Genetics Center (supported by the National Institutes of Health [NIH], Office of Research Infrastructure Programs [P40 OD010440]); the *C. elegans* Reverse Genetics Core Facility at the University of British Columbia, which is part of the International *C. elegans* Gene Knockout Consortium; and Shohei Mitani (Tokyo Women’s Medical University, Tokyo, Japan) for nematode strains. We thank Bill Schafer (MRC Laboratory of Molecular Biology) for kindly providing us with their *connexin 36* construct.⁸⁴ The diagrams used in the figures are modified versions of diagrams provided by Z. Altun (www.wormatlas.org) and BioRender (<https://app.biorender.com/>; D.A.C.-R. [2024] <https://BioRender.com/j08h349>). We thank Aravi Samuel (Harvard University) for generous assistance with technical knowledge in the development of behavioral rigs and calcium-imaging platforms. We thank Hari Shroff (Janelia Research Campus) and Andrew Lauzier (University of Maryland) for image processing codes used for videos of freely moving animals. The work in Z.-W.W.’s lab was supported by R01NS109388 and R01MH085927. Research in the D.A.C.-R. lab was supported by NIH R01NS076558, National

Science Foundation (NSF IOS 1353845), DP1NS111778, and an HHMI Scholar Award.

AUTHOR CONTRIBUTIONS

A.C.C. identified the behavioral phenotype of *inx-1*-mutant animals resulting in abnormal isothermal tracking and identified the AIY neurons as the site of action via a subtractive labeling strategy and the generation of a conditional knockout strain for the *inx-1* gene. A.A.-P. performed the original genetic screen that isolated the *ola375* allele and identified the *ola375* allele as a genetic lesion in the *inx-1* gene, performed characterization and analyses of the behavioral phenotypes associated with *inx-1* mutants, performed and analyzed calcium-imaging experiments in immobilized animals when presented with temperature stimuli, and performed and analyzed behavioral suppression experiments using mammalian Cx36 gap junction constructs. J.B. performed the modeling experiments. M.D.G. performed dispersion assays, calcium-imaging experiments, and analyses and assisted with all the revisions. L.N. performed and analyzed the electrophysiological experiments. I.R., E.M.W., and J.D.H. assisted in experimental design, data acquisition, and analysis. A.A.-P. and D.A.C.-R. prepared the manuscript with the assistance of all authors, in particular Z.W.-W., J.B., and M.D.G.

DECLARATION OF INTERESTS

The authors declare no competing interests.

STAR METHODS

Detailed methods are provided in the online version of this paper and include the following:

- KEY RESOURCES TABLE
- EXPERIMENTAL MODEL AND STUDY PARTICIPANT DETAILS
 - *C. elegans*
- METHOD DETAILS
 - Molecular biology
 - Nematode Strains and maintenance
 - Genotyping of mutant strains
 - Generation of transgenic strains
 - Sensitized forward-genetic screens
 - Identification of *ola375* causative lesions
 - Generation of “floxed” *inx-1(ola278)* for conditional Knock-Out experiments
 - Complementation Assays
 - Thermotaxis Behavioral Assays
 - Shallow gradients for Gradient Migration Quantification
 - Moderate and steep gradients for Isothermal Tracking Quantification
 - Dispersion Assays
 - Confocal imaging
 - Calcium Imaging
 - Electrophysiological experiment and analyses
- QUANTIFICATION AND STATISTICAL ANALYSIS
 - Statistical Tests
 - Quantification of isothermal tracking
 - Quantification of behavior
 - Quantification of calcium imaging in AIY

SUPPLEMENTAL INFORMATION

Supplemental information can be found online at <https://doi.org/10.1016/j.cell.2024.11.037>.

Received: November 17, 2023

Revised: July 26, 2024

Accepted: November 27, 2024

Published: December 31, 2024

REFERENCES

- Murakami, H., Bessinger, K., Hellmann, J., and Murakami, S. (2005). Ageing-dependent and -independent modulation of associative learning behavior by insulin/insulin-like growth factor-1 signal in *Caenorhabditis elegans*. *J. Neurosci.* 25, 10894–10904. <https://doi.org/10.1523/JNEUROSCI.3600-04.2005>.
- Faumont, S., Lindsay, T.H., and Lockery, S.R. (2012). Neuronal microcircuits for decision making in *C. elegans*. *Curr. Opin. Neurobiol.* 22, 580–591. <https://doi.org/10.1016/j.conb.2012.05.005>.
- Collins, K.M., and Koelle, M.R. (2013). Postsynaptic ERG potassium channels limit muscle excitability to allow distinct egg-laying behavior states in *Caenorhabditis elegans*. *J. Neurosci.* 33, 761–775. <https://doi.org/10.1523/JNEUROSCI.3896-12.2013>.
- Satoh, Y., Sato, H., Kunitomo, H., Fei, X., Hashimoto, K., and Iino, Y. (2014). Regulation of experience-dependent bidirectional chemotaxis by a neural circuit switch in *Caenorhabditis elegans*. *J. Neurosci.* 34, 15631–15637. <https://doi.org/10.1523/JNEUROSCI.1757-14.2014>.
- Collins, K.M., Bode, A., Fernandez, R.W., Tanis, J.E., Brewer, J.C., Creamer, M.S., and Koelle, M.R. (2016). Activity of the *C. elegans* egg-laying behavior circuit is controlled by competing activation and feedback inhibition. *eLife* 5, e21126. <https://doi.org/10.7554/eLife.21126>.
- Guillermín, M.L., Carrillo, M.A., and Hallem, E.A. (2017). A Single Set of Interneurons Drives Opposite Behaviors in *C. elegans*. *Curr. Biol.* 27, 2630–2639.e6. <https://doi.org/10.1016/j.cub.2017.07.023>.
- Hampel, S., McKellar, C.E., Simpson, J.H., and Seeds, A.M. (2017). Simultaneous activation of parallel sensory pathways promotes a grooming sequence in *Drosophila*. *eLife* 6, e28804. <https://doi.org/10.7554/eLife.28804>.
- Amin, H., and Lin, A.C. (2019). Neuronal mechanisms underlying innate and learned olfactory processing in *Drosophila*. *Curr. Opin. Insect Sci.* 36, 9–17. <https://doi.org/10.1016/j.cois.2019.06.003>.
- Grunwald-Kadow, I.C. (2019). State-dependent plasticity of innate behavior in fruit flies. *Curr. Opin. Neurobiol.* 54, 60–65. <https://doi.org/10.1016/j.conb.2018.08.014>.
- Wang, Y., Zhang, X., Xin, Q., Hung, W., Florman, J., Huo, J., Xu, T., Xie, Y., Alkema, M.J., Zhen, M., et al. (2020). Flexible motor sequence generation during stereotyped escape responses. *eLife* 9, e56942. <https://doi.org/10.7554/eLife.56942>.
- Ikeda, M., Nakano, S., Giles, A.C., Xu, L., Costa, W.S., Gottschalk, A., and Mori, I. (2020). Context-dependent operation of neural circuits underlies a navigation behavior in *Caenorhabditis elegans*. *Proc. Natl. Acad. Sci. USA* 117, 6178–6188. <https://doi.org/10.1073/pnas.1918528117>.
- Dal Bello, M., Pérez-Escudero, A., Schroeder, F.C., and Gore, J. (2021). Inversion of pheromone preference optimizes foraging in *C. elegans*. *eLife* 10, e58144. <https://doi.org/10.7554/eLife.58144>.
- Tao, L., and Bhandawat, V. (2022). Mechanisms of Variability Underlying Odor-Guided Locomotion. *Front. Behav. Neurosci.* 16, 871884. <https://doi.org/10.3389/fnbeh.2022.871884>.
- Hiroki, S., Yoshitane, H., Mitsui, H., Sato, H., Umatani, C., Kanda, S., Fukada, Y., and Iino, Y. (2022). Molecular encoding and synaptic decoding of context during salt chemotaxis in *C. elegans*. *Nat. Commun.* 13, 2928. <https://doi.org/10.1038/s41467-022-30279-7>.
- Yang, W., Wu, T., Tu, S., Qin, Y., Shen, C., Li, J., Choi, M.K., Duan, F., and Zhang, Y. (2022). Redundant neural circuits regulate olfactory integration. *PLoS Genet.* 18, e1010029. <https://doi.org/10.1371/journal.pgen.1010029>.
- Huda, R., Goard, M.J., Pho, G.N., and Sur, M. (2019). Neural mechanisms of sensorimotor transformation and action selection. *Eur. J. Neurosci.* 49, 1055–1060. <https://doi.org/10.1111/ejn.14069>.
- Takagi, S., and Nose, A. (2019). Circuit architecture for somatotopic action selection in invertebrates. *Neurosci. Res.* 140, 37–42. <https://doi.org/10.1016/j.neures.2018.08.008>.
- Hulse, B.K., Haberkern, H., Franconville, R., Turner-Evans, D., Take-mura, S.Y., Wolff, T., Noorman, M., Dreher, M., Dan, C., Parekh, R., et al. (2021). A connectome of the *Drosophila* central complex reveals network motifs suitable for flexible navigation and context-dependent action selection. *eLife* 10, e66039. <https://doi.org/10.7554/eLife.66039>.
- Hedgecock, E.M., and Russell, R.L. (1975). Normal and mutant thermotaxis in the nematode *Caenorhabditis elegans*. *Proc. Natl. Acad. Sci. USA* 72, 4061–4065. <https://doi.org/10.1073/pnas.72.10.4061>.
- Skerrett, I.M., and Williams, J.B. (2017). A structural and functional comparison of gap junction channels composed of connexins and innexins. *Dev. Neurobiol.* 77, 522–547. <https://doi.org/10.1002/dneu.22447>.
- Sánchez, A., Castro, C., Flores, D.L., Gutiérrez, E., and Baldi, P. (2019). Gap Junction Channels of Innexins and Connexins: Relations and Computational Perspectives. *Int. J. Mol. Sci.* 20, 2476. <https://doi.org/10.3390/ijms20102476>.
- Luo, L., Clark, D.A., Biron, D., Mahadevan, L., and Samuel, A.D.T. (2006). Sensorimotor control during isothermal tracking in *Caenorhabditis elegans*. *J. Exp. Biol.* 209, 4652–4662. <https://doi.org/10.1242/jeb.02590>.
- Mori, I., and Ohshima, Y. (1995). Neural regulation of thermotaxis in *Caenorhabditis elegans*. *Nature* 376, 344–348. <https://doi.org/10.1038/376344a0>.
- Robert, O., Mori, I., Yamashita, Y., Honda, H., Ohshima, Y., Liu, Y., and Ruvkun, G. (1997). Regulation of interneuron function in the *C. elegans* thermoregulatory pathway by the *tx-3* LIM homeobox gene. *Neuron* 19, 345–357. [https://doi.org/10.1016/s0896-6273\(00\)80944-7](https://doi.org/10.1016/s0896-6273(00)80944-7).
- Satterlee, J.S., Sasakura, H., Kuhara, A., Berkeley, M., Mori, I., and SenGupta, P. (2001). Specification of thermosensory neuron fate in *C. elegans* requires *tx-1*, a homolog of *otd/Otx*. *Neuron* 31, 943–956. [https://doi.org/10.1016/s0896-6273\(01\)00431-7](https://doi.org/10.1016/s0896-6273(01)00431-7).
- Chung, S.H., Clark, D.A., Gabel, C.V., Mazur, E., and Samuel, A.D.T. (2006). The role of the AFD neuron in *C. elegans* thermotaxis analyzed using femtosecond laser ablation. *BMC Neurosci.* 7, 30. <https://doi.org/10.1186/1471-2202-7-30>.
- Clark, D.A., Biron, D., SenGupta, P., and Samuel, A.D.T. (2006). The AFD sensory neurons encode multiple functions underlying thermotactic behavior in *Caenorhabditis elegans*. *J. Neurosci.* 26, 7444–7451. <https://doi.org/10.1523/JNEUROSCI.1137-06.2006>.
- Biron, D., Wasserman, S., Thomas, J.H., Samuel, A.D.T., and SenGupta, P. (2008). An olfactory neuron responds stochastically to temperature and modulates *Caenorhabditis elegans* thermotactic behavior. *Proc. Natl. Acad. Sci. USA* 105, 11002–11007. <https://doi.org/10.1073/pnas.0805004105>.
- Kuhara, A., Okumura, M., Kimata, T., Tanizawa, Y., Takano, R., Kimura, K.D., Inada, H., Matsumoto, K., and Mori, I. (2008). Temperature sensing by an olfactory neuron in a circuit controlling behavior of *C. elegans*. *Science* 320, 803–807. <https://doi.org/10.1126/science.1148922>.
- Beverly, M., Anbil, S., and SenGupta, P. (2011). Degeneracy and neuro-modulation among thermosensory neurons contribute to robust thermo-sensory behaviors in *Caenorhabditis elegans*. *J. Neurosci.* 31, 11718–11727. <https://doi.org/10.1523/JNEUROSCI.1098-11.2011>.
- Matsuyama, H.J., and Mori, I. (2020). Neural Coding of Thermal Preferences in the Nematode *Caenorhabditis elegans*. *eNeuro* 7, ENEURO.0414-19.2020. <https://doi.org/10.1523/ENEURO.0414-19.2020>.
- White, J.G., Southgate, E., Thomson, J.N., and Brenner, S. (1986). The structure of the nervous system of the nematode *Caenorhabditis elegans*. *Philos. Trans. R. Soc. Lond. B Biol. Sci.* 314, 1–340. <https://doi.org/10.1098/rstb.1986.0056>.

33. Ramot, D., MacInnis, B.L., and Goodman, M.B. (2008). Bidirectional temperature-sensing by a single thermosensory neuron in *C. elegans*. *Nat. Neurosci.* 11, 908–915. <https://doi.org/10.1038/nn.2157>.
34. Goodman, M.B., and SenGupta, P. (2018). The extraordinary AFD thermosensor of *C. elegans*. *Pflugers Arch.* 470, 839–849. <https://doi.org/10.1007/s00424-017-2089-5>.
35. Tsalik, E.L., and Hobert, O. (2003). Functional mapping of neurons that control locomotory behavior in *Caenorhabditis elegans*. *J. Neurobiol.* 56, 178–197. <https://doi.org/10.1002/neu.10245>.
36. Gray, J.M., Hill, J.J., and Bargmann, C.I. (2005). A circuit for navigation in *Caenorhabditis elegans*. *Proc. Natl. Acad. Sci. USA* 102, 3184–3191. <https://doi.org/10.1073/pnas.0409009102>.
37. Chalasani, S.H., Chronis, N., Tsunozaki, M., Gray, J.M., Ramot, D., Goodman, M.B., and Bargmann, C.I. (2007). Dissecting a circuit for olfactory behaviour in *Caenorhabditis elegans*. *Nature* 450, 63–70. <https://doi.org/10.1038/nature06292>.
38. Kocabas, A., Shen, C.H., Guo, Z.V., and Ramanathan, S. (2012). Controlling interneuron activity in *Caenorhabditis elegans* to evoke chemotactic behaviour. *Nature* 490, 273–277. <https://doi.org/10.1038/nature11431>.
39. Li, Z., Liu, J., Zheng, M., and Xu, X.Z.S. (2014). Encoding of both analog-and digital-like behavioral outputs by one *C. elegans* interneuron. *Cell* 159, 751–765. <https://doi.org/10.1016/j.cell.2014.09.056>.
40. Liu, H., Yang, W., Wu, T., Duan, F., Soucy, E., Jin, X., and Zhang, Y. (2018). Cholinergic Sensorimotor Integration Regulates Olfactory Steering. *Neuron* 97, 390–405.e3. <https://doi.org/10.1016/j.neuron.2017.12.003>.
41. Kuhara, A., Ohnishi, N., Shimowada, T., and Mori, I. (2011). Neural coding in a single sensory neuron controlling opposite seeking behaviours in *Caenorhabditis elegans*. *Nat. Commun.* 2, 355. <https://doi.org/10.1038/ncomms1352>.
42. Luo, L., Cook, N., Venkatachalam, V., Martinez-Velazquez, L.A., Zhang, X., Calvo, A.C., Hawk, J., MacInnis, B.L., Frank, M., Ng, J.H.R., et al. (2014). Bidirectional thermotaxis in *Caenorhabditis elegans* is mediated by distinct sensorimotor strategies driven by the AFD thermosensory neurons. *Proc. Natl. Acad. Sci. U. S. A.* 111, 2776–2781. <https://doi.org/10.1073/pnas.1315205111>.
43. Davis, M.W., Hammarlund, M., Harrach, T., Hullett, P., Olsen, S., and Jorgensen, E.M. (2005). Rapid single nucleotide polymorphism mapping in *C. elegans*. *BMC Genomics* 6, 118. <https://doi.org/10.1186/1471-2164-6-118>.
44. Doitsidou, M., Poole, R.J., Sarin, S., Bigelow, H., and Hobert, O. (2010). *C. elegans* mutant identification with a one-step whole-genome sequencing and SNP mapping strategy. *PLoS One* 5, e15435. <https://doi.org/10.1371/journal.pone.0015435>.
45. Zuryn, S., Le Gras, S., Jamet, K., and Jarriault, S. (2010). A strategy for direct mapping and identification of mutations by whole-genome sequencing. *Genetics* 186, 427–430. <https://doi.org/10.1534/genetics.110.119230>.
46. Minevich, G., Park, D.S., Blankenberg, D., Poole, R.J., and Hobert, O. (2012). CloudMap: a cloud-based pipeline for analysis of mutant genome sequences. *Genetics* 192, 1249–1269. <https://doi.org/10.1534/genetics.112.144204>.
47. Collet, J., Spike, C.A., Lundquist, E.A., Shaw, J.E., and Herman, R.K. (1998). Analysis of osm-6, a gene that affects sensory cilium structure and sensory neuron function in *Caenorhabditis elegans*. *Genetics* 148, 187–200. <https://doi.org/10.1093/genetics/148.1.187>.
48. Chou, J.H., Bargmann, C.I., and SenGupta, P. (2001). The *Caenorhabditis elegans* odr-2 gene encodes a novel Ly-6-related protein required for olfaction. *Genetics* 157, 211–224. <https://doi.org/10.1093/genetics/157.1.211>.
49. Goodenough, D.A., Goliger, J.A., and Paul, D.L. (1996). Connexins, connexons, and intercellular communication. *Annu. Rev. Biochem.* 65, 475–502. <https://doi.org/10.1146/annurev.bi.65.070196.002355>.
50. Phelan, P., Bacon, J.P., Davies, J.A., Stebbings, L.A., Todman, M.G., Avery, L., Baines, R.A., Barnes, T.M., Ford, C., Hekimi, S., et al. (1998). Innexins: a family of invertebrate gap-junction proteins. *Trends Genet.* 14, 348–349. [https://doi.org/10.1016/s0168-9525\(98\)01547-9](https://doi.org/10.1016/s0168-9525(98)01547-9).
51. Bao, L., Samuels, S., Locovei, S., Macagno, E.R., Muller, K.J., and Dahl, G. (2007). Innexins form two types of channels. *FEBS Lett.* 571, 5703–5708. <https://doi.org/10.1016/j.febslet.2007.11.030>.
52. Cheung, G., Chever, O., and Rouach, N. (2014). Connexons and pannexons: newcomers in neurophysiology. *Front. Cell. Neurosci.* 8, 348. <https://doi.org/10.3389/fncel.2014.00348>.
53. Palacios-Prado, N., Huettner, W., and Pereda, A.E. (2014). Hemichannel composition and electrical synaptic transmission: molecular diversity and its implications for electrical rectification. *Front. Cell. Neurosci.* 8, 324. <https://doi.org/10.3389/fncel.2014.00324>.
54. Curti, S., Davoine, F., and Dapino, A. (2022). Function and Plasticity of Electrical Synapses in the Mammalian Brain: Role of Non-Junctional Mechanisms. *Biology (Basel)* 11, 81. <https://doi.org/10.3390/biology11010081>.
55. Starich, T., Sheehan, M., Jadrich, J., and Shaw, J. (2001). Innexins in *C. elegans*. *Cell Commun. Adhes.* 8, 311–314. <https://doi.org/10.3109/15419060109080744>.
56. Bauer, R., Löer, B., Ostrowski, K., Martini, J., Weimbs, A., Lechner, H., and Hoch, M. (2005). Intercellular communication: the *Drosophila* innixin multiprotein family of gap junction proteins. *Chem. Biol.* 12, 515–526. <https://doi.org/10.1016/j.chembiol.2005.02.013>.
57. Starich, T.A., Xu, J., Skerrett, I.M., Nicholson, B.J., and Shaw, J.E. (2009). Interactions between innexins UNC-7 and UNC-9 mediate electrical synapse specificity in the *Caenorhabditis elegans* locomotory nervous system. *Neural Dev.* 4, 16. <https://doi.org/10.1186/1749-8104-4-16>.
58. Oshima, A., Matsuzawa, T., Nishikawa, K., and Fujiyoshi, Y. (2013). Oligomeric structure and functional characterization of *Caenorhabditis elegans* Innixin-6 gap junction protein. *J. Biol. Chem.* 288, 10513–10521. <https://doi.org/10.1074/jbc.M112.428383>.
59. Hall, D.H. (2017). Gap junctions in *C. elegans*: Their roles in behavior and development. *Dev. Neurobiol.* 77, 587–596. <https://doi.org/10.1002/dneu.22408>.
60. Jang, H., Levy, S., Flavell, S.W., Mende, F., Latham, R., Zimmer, M., and Bargmann, C.I. (2017). Dissection of neuronal gap junction circuits that regulate social behavior in *Caenorhabditis elegans*. *Proc. Natl. Acad. Sci. USA* 114, E1263–E1272. <https://doi.org/10.1073/pnas.1621274114>.
61. Jin, E.J., Park, S., Lyu, X., and Jin, Y. (2020). Gap junctions: historical discoveries and new findings in the *Caenorhabditis elegans* nervous system. *Biol. Open* 9, bio053983. <https://doi.org/10.1242/bio.053983>.
62. Walker, D.S., and Schafer, W.R. (2020). Distinct roles for innixin gap junctions and hemichannels in mechanosensation. *eLife* 9, e50597. <https://doi.org/10.7554/eLife.50597>.
63. Altun, Z.F., Chen, B., Wang, Z.W., and Hall, D.H. (2009). High resolution map of *Caenorhabditis elegans* gap junction proteins. *Dev. Dyn.* 238, 1936–1950. <https://doi.org/10.1002/dvdy.22025>.
64. Bhattacharya, A., Aghayeva, U., Berghoff, E.G., and Hobert, O. (2019). Plasticity of the Electrical connectome of *C. elegans*. *Cell* 176, 1174–1189.e16. <https://doi.org/10.1016/j.cell.2018.12.024>.
65. Liu, P., Chen, B., Altun, Z.F., Gross, M.J., Shan, A., Schuman, B., Hall, D.H., and Wang, Z.W. (2013). Six innexins contribute to electrical coupling of *C. elegans* body-wall muscle. *PLoS One* 8, e76877. <https://doi.org/10.1371/journal.pone.0076877>.
66. Choi, U., Wang, H., Hu, M., Kim, S., and Sieburth, D. (2021). Presynaptic coupling by electrical synapses coordinates a rhythmic behavior by synchronizing the activities of a neuron pair. *Proc. Natl. Acad. Sci. USA* 118, e2022599118. <https://doi.org/10.1073/pnas.2022599118>.
67. Jiang, J., Su, Y., Zhang, R., Li, H., Tao, L., and Liu, Q. (2022). *C. elegans* enteric motor neurons fire synchronized action potentials underlying the

- defecation motor program. *Nat. Commun.* 13, 2783. <https://doi.org/10.1038/s41467-022-30452-y>.
68. Dickinson, D.J., Pani, A.M., Heppert, J.K., Higgins, C.D., and Goldstein, B. (2015). Streamlined Genome Engineering with a Self-Excising Drug Selection Cassette. *Genetics* 200, 1035–1049. <https://doi.org/10.1534/genetics.115.178335>.
 69. Hubbard, E.J.A. (2014). FLP/FRT and Cre/lox recombination technology in *C. elegans*. *Methods* 68, 417–424. <https://doi.org/10.1016/j.ymeth.2014.05.007>.
 70. Hawk, J.D., Calvo, A.C., Liu, P., Almoril-Porras, A., Aljobeh, A., Torruella-Suárez, M.L., Ren, I., Cook, N., Greenwood, J., Luo, L., et al. (2018). Integration of Plasticity Mechanisms within a Single Sensory Neuron of *C. elegans* Actuates a Memory. *Neuron* 97, 356–367.e4. <https://doi.org/10.1016/j.neuron.2017.12.027>.
 71. Narayan, A., Laurent, G., and Sternberg, P.W. (2011). Transfer characteristics of a thermosensory synapse in *Caenorhabditis elegans*. *Proc. Natl. Acad. Sci. USA* 108, 9667–9672. <https://doi.org/10.1073/pnas.1106617108>.
 72. Gomez, M., De Castro, E., Guarin, E., Sasakura, H., Kuhara, A., Mori, I., Bartfai, T., Bargmann, C.I., and Nef, P. (2001). Ca²⁺ signaling via the neuronal calcium sensor-1 regulates associative learning and memory in *C. elegans*. *Neuron* 30, 241–248. [https://doi.org/10.1016/s0896-6273\(01\)00276-8](https://doi.org/10.1016/s0896-6273(01)00276-8).
 73. Witvliet, D., Mulcahy, B., Mitchell, J.K., Meirovitch, Y., Berger, D.R., Wu, Y., Liu, Y., Koh, W.X., Parvathala, R., Holmyard, D., et al. (2021). Connectomes across development reveal principles of brain maturation. *Nature* 596, 257–261. <https://doi.org/10.1038/s41586-021-03778-8>.
 74. Ji, N., Venkatachalam, V., Rodgers, H.D., Hung, W., Kawano, T., Clark, C.M., Lim, M., Alkema, M.J., Zhen, M., and Samuel, A.D. (2021). Corollary discharge promotes a sustained motor state in a neural circuit for navigation. *eLife* 10, e68848. <https://doi.org/10.7554/eLife.68848>.
 75. Colón-Ramos, D.A., Margeta, M.A., and Shen, K. (2007). Glia promote local synaptogenesis through UNC-6 (netrin) signaling in *C. elegans*. *Science* 318, 103–106. <https://doi.org/10.1126/science.1143762>.
 76. Liu, Q., Kidd, P.B., Dobosiewicz, M., and Bargmann, C.I. (2018). *C. elegans* AWA Olfactory Neurons Fire Calcium-Mediated All-or-None Action Potentials. *Cell* 175, 57–70.e17. <https://doi.org/10.1016/j.cell.2018.08.018>.
 77. Wenick, A.S., and Hobert, O. (2004). Genomic cis-regulatory architecture and trans-acting regulators of a single interneuron-specific gene battery in *C. elegans*. *Dev. Cell* 6, 757–770. <https://doi.org/10.1016/j.devcel.2004.05.004>.
 78. Bloomfield, S.A., and Dacheux, R.F. (2001). Rod vision: pathways and processing in the mammalian retina. *Prog. Retin. Eye Res.* 20, 351–384. [https://doi.org/10.1016/s1350-9462\(00\)00031-8](https://doi.org/10.1016/s1350-9462(00)00031-8).
 79. Masland, R.H. (2001). The fundamental plan of the retina. *Nat. Neurosci.* 4, 877–886. <https://doi.org/10.1038/nn0901-877>.
 80. Hanson, L., Ravi-Chander, P., Berson, D., and Awatramani, G.B. (2023). Hierarchical retinal computations rely on hybrid chemical-electrical signaling. *Cell Rep.* 42, 112030. <https://doi.org/10.1016/j.celrep.2023.112030>.
 81. Alcamí, P., and Pereda, A.E. (2019). Beyond plasticity: the dynamic impact of electrical synapses on neural circuits. *Nat. Rev. Neurosci.* 20, 253–271. <https://doi.org/10.1038/s41583-019-0133-5>.
 82. Wakabayashi, T., Kitagawa, I., and Shingai, R. (2004). Neurons regulating the duration of forward locomotion in *Caenorhabditis elegans*. *Neurosci. Res.* 50, 103–111. <https://doi.org/10.1016/j.neures.2004.06.005>.
 83. Phelan, P. (2005). Innexins: members of an evolutionarily conserved family of gap-junction proteins. *Biochim. Biophys. Acta* 1711, 225–245. <https://doi.org/10.1016/j.bbamem.2004.10.004>.
 84. Rabinowitch, I., Chatzigeorgiou, M., Zhao, B., Treinin, M., and Schafer, W.R. (2014). Rewiring neural circuits by the insertion of ectopic electrical synapses in transgenic *C. elegans*. *Nat. Commun.* 5, 4442. <https://doi.org/10.1038/ncomms5442>.
 85. Rabinowitch, I., Colón-Ramos, D.A., and Krieg, M. (2024). Understanding neural circuit function through synaptic engineering. *Nat. Rev. Neurosci.* 25, 131–139. <https://doi.org/10.1038/s41583-023-00777-8>.
 86. Bouhours, M., Po, M.D., Gao, S., Hung, W., Li, H., Georgiou, J., Roder, J.C., and Zhen, M. (2011). A co-operative regulation of neuronal excitability by UNC-7 innexin and NCA/NALCN leak channel. *Mol. Brain* 4, 16. <https://doi.org/10.1186/1756-6606-4-16>.
 87. Correa, P.A., Gruninger, T., and García, L.R. (2015). DOP-2 D2-Like Receptor Regulates UNC-7 Innexins to Attenuate Recurrent Sensory Motor Neurons during *C. elegans* Copulation. *J. Neurosci.* 35, 9990–10004. <https://doi.org/10.1523/JNEUROSCI.0940-15.2015>.
 88. Liu, P., Chen, B., Mailler, R., and Wang, Z.W. (2017). Antidromic-rectifying gap junctions amplify chemical transmission at functionally mixed electrical-chemical synapses. *Nat. Commun.* 8, 14818. <https://doi.org/10.1038/ncomms14818>.
 89. Voelker, L., Upadhyaya, B., Ferkey, D.M., Woldemariam, S., L'Etoile, N.D., Rabinowitch, I., and Bai, J. (2019). INX-18 and INX-19 play distinct roles in electrical synapses that modulate aversive behavior in *Caenorhabditis elegans*. *PLoS Genet.* 15, e1008341. <https://doi.org/10.1371/journal.pgen.1008341>.
 90. Choi, M.K., Liu, H., Wu, T., Yang, W., and Zhang, Y. (2020). NMDAR-mediated modulation of gap junction circuit regulates olfactory learning in *C. elegans*. *Nat. Commun.* 11, 3467. <https://doi.org/10.1038/s41467-020-17218-0>.
 91. Chatzigeorgiou, M., and Schafer, W.R. (2011). Lateral facilitation between primary mechanosensory neurons controls nose touch perception in *C. elegans*. *Neuron* 70, 299–309. <https://doi.org/10.1016/j.neuron.2011.02.046>.
 92. Macosko, E.Z., Pokala, N., Feinberg, E.H., Chalasani, S.H., Butcher, R.A., Clardy, J., and Bargmann, C.I. (2009). A hub-and-spoke circuit drives pheromone attraction and social behaviour in *C. elegans*. *Nature* 458, 1171–1175. <https://doi.org/10.1038/nature07886>.
 93. Liu, P., Chen, B., and Wang, Z.W. (2020). GABAergic motor neurons bias locomotor decision-making in *C. elegans*. *Nat. Commun.* 11, 5076. <https://doi.org/10.1038/s41467-020-18893-9>.
 94. Gershoff, M., Berck, M., Mathew, D., Luo, L., Kane, E.A., Carlson, J.R., and Samuel, A.D.T. (2012). Controlling airborne cues to study small animal navigation. *Nat. Methods* 9, 290–296. <https://doi.org/10.1038/nmeth.1853>.
 95. Schindelin, J., Arganda-Carreras, I., Frise, E., Kaynig, V., Longair, M., Pietzsch, T., Preibisch, S., Rueden, C., Saalfeld, S., Schmid, B., et al. (2012). Fiji: an open-source platform for biological-image analysis. *Nat. Methods* 9, 676–682. <https://doi.org/10.1038/nmeth.2019>.
 96. Ershov, D., Phan, M.S., Pylyváriinen, J.W., Rigaud, S.U., Le Blanc, L., Charles-Orszag, A., Conway, J.R.W., Laine, R.F., Roy, N.H., Bonazzi, D., et al. (2022). TrackMate 7: integrating state-of-the-art segmentation algorithms into tracking pipelines. *Nat. Methods* 19, 829–832. <https://doi.org/10.1038/s41592-022-01507-1>.
 97. Edelstein, A.D., Tsuchida, M.A., Amodaj, N., Pinkard, H., Vale, R.D., and Stuurman, N. (2014). Advanced methods of microscope control using μManager software. *J. Biol. Methods* 1, 1. <https://doi.org/10.14440/jbm.2014.36>.
 98. Brenner, S. (1974). The genetics of *Caenorhabditis elegans*. *Genetics* 77, 71–94. <https://doi.org/10.1093/genetics/77.1.71>.
 99. Merritt, C., and Seydoux, G. (2010). Transgenic solutions for the germline. *WormBook* 1–21, 1–21. <https://doi.org/10.1895/wormbook.1.148.1>.
 100. Mello, C., and Fire, A. (1995). DNA transformation. *Methods Cell Biol.* 48, 451–482. [https://doi.org/10.1016/S0091-679X\(08\)61399-0](https://doi.org/10.1016/S0091-679X(08)61399-0).

101. Okochi, Y., Kimura, K.D., Ohta, A., and Mori, I. (2005). Diverse regulation of sensory signaling by *C. elegans* nPKC-epsilon/eta TTX-4. *EMBO J.* 24, 2127–2137. <https://doi.org/10.1038/sj.emboj.7600697>.
102. Stiernagle, T. (2006). Maintenance of *C. elegans*. *WormBook* 1–11, 1–11. <https://doi.org/10.1895/wormbook.1.101.1>.
103. Goodman, M.B., Klein, M., Lasse, S., Luo, L., Mori, I., Samuel, A., Sen-Gupta, P., and Wang, D. (2014). Thermotaxis navigation behavior. *WormBook* 1–10, 1–10. <https://doi.org/10.1895/wormbook.1.168.1>.
104. Kimura, K.D., Miyawaki, A., Matsumoto, K., and Mori, I. (2004). The *C. elegans* thermosensory neuron AFD responds to warming. *Curr. Biol.* 14, 1291–1295. <https://doi.org/10.1016/j.cub.2004.06.060>.

STAR★METHODS

KEY RESOURCES TABLE

REAGENT or RESOURCE	SOURCE	IDENTIFIER
Deposited data		
GitHub: https://doi.org/10.5281/zenodo.14170612	This paper	GitHub: https://doi.org/10.5281/zenodo.14170612
Experimental models: Organisms/strains		
<i>C. elegans</i> : Strain N2: Bristol wild-type strain	Caenorhabditis Genetics Center	N2
<i>C. elegans</i> : Strain DCR7342: <i>inx-1(ola375)</i> <i>X</i> outcrossed 1 time	This paper	DCR Lab Strain ID: DCR7342
<i>C. elegans</i> : Strain DCR5281: <i>inx-1(tm3524)</i> <i>X</i> outcrossed 6 times	This paper	DCR Lab Strain ID: DCR5281
<i>C. elegans</i> : Strain DCR5283: <i>inx-1(gk580946)</i> <i>X</i> outcrossed 4 times	This paper	DCR Lab Strain ID: DCR5283
<i>C. elegans</i> : Strain CB4856 Hawaiian wild-type strain	Caenorhabditis Genetics Center	CB4856
<i>C. elegans</i> : Strain DCR3542: <i>pkc-1(nj1) V; inx-1(ola375) X</i>	This paper	DCR Lab Strain ID: DCR3542
<i>C. elegans</i> : Strain IK105: <i>pkc-1(nj1) V</i>	Caenorhabditis Genetics Center	IK105
<i>C. elegans</i> : Strain FX03524: <i>inx-1(tm3524) X</i>	Shohei Mitani/ NBRP	FX03524
<i>C. elegans</i> : Strain FX16643: <i>tmls1091[Ptx-3::nCRE, Plin-44::GFP]</i>	Shohei Mitani/ NBRP	FX16643
<i>C. elegans</i> : Strain DCR3682: <i>inx-1(tm3524) X; olaEx2136[Pinx-1(2.5kb)::INX-1gene::SL2::GFP (10 ng/ul), Punc-122::RFP (35 ng/ul)]</i>	This paper	DCR Lab Strain ID: DCR3682
<i>C. elegans</i> : Strain DCR4453: <i>inx-1(tm3524) X; olaEx2619[Pmod-1::INX1AcDNA+ INX1BcDNA::SL2::GFP (10ng/mL each); Punc122::GFP] Line 2</i>	This paper	DCR Lab Strain ID: DCR4453
<i>C. elegans</i> : Strain DCR4116: <i>olaEx2390[Pinx-1(2.5kb)::GFP, Pinx-1(1.5kb)::mCherry, Punc-122::GFP]</i>	This paper	DCR Lab Strain ID: DCR4116
<i>C. elegans</i> : Strain DCR4708: <i>inx-1(ola278) X</i>	This paper	DCR Lab Strain ID: DCR4708
<i>C. elegans</i> : Strain DCR4997: <i>inx-1(ola278) X, 3 times outcrossed with N2</i>	This paper	DCR Lab Strain ID: DCR4997
<i>C. elegans</i> : Strain DCR4984: <i>inx-1(ola278) X; olaEx2943 [Pinx-1(2.5kb)::nCRE (25 ng/ul), Punc-122::RFP] Line 1</i>	This paper	DCR Lab Strain ID: DCR4984
<i>C. elegans</i> : Strain DCR4985: <i>inx-1(ola278) X; olaEx2944 [Pinx-1(2.5kb)::nCRE::3UTR; Punc122::RFP] Line 2</i>	This paper	DCR Lab Strain ID: DCR4985
<i>C. elegans</i> : Strain DCR4986: <i>inx-1(ola278) X; olaEx2945 [Pinx-1(2.5kb)::nCRE::3UTR; Punc122::RFP] Line 3</i>	This paper	DCR Lab Strain ID: DCR4986
<i>C. elegans</i> : Strain DCR4990: <i>inx-1(ola278) X; olaEx2949 [Pinx-1(1kb)::nCRE (25 ng/ul), Punc-122::RFP] Line 1</i>	This paper	DCR Lab Strain ID: DCR4990
<i>C. elegans</i> : Strain DCR4991: <i>inx-1(ola278) X; olaEx2950[Pinx-1(1kb)::nCRE::3UTR (25 ng/ul), Punc-122::RFP] Line 2</i>	This paper	DCR Lab Strain ID: DCR4991
<i>C. elegans</i> : Strain DCR4992: <i>inx-1(ola278) X; olaEx2951 [Pinx-1(1kb)::Ncre::3UTR (25 ng/ul), Punc-122::RFP] Line 3</i>	This paper	DCR Lab Strain ID: DCR4992
<i>C. elegans</i> : Strain DCR4993: <i>inx-1(ola278) X; olaEx2952 [Pinx-1(1kb)::Ncre::3UTR (25 ng/ul), Punc-122::RFP] Line 4</i>	This paper	DCR Lab Strain ID: DCR4993
<i>C. elegans</i> : Strain DCR5027: <i>inx-1(ola278) X; olaEx2976 [Pcex-1::nCRE::3UTR (25 ng/ul), Punc-122::RFP] Line 1</i>	This paper	DCR Lab Strain ID: DCR5027
<i>C. elegans</i> : Strain DCR5028: <i>inx-1(ola278) X; olaEx2977 [Pcex-1::nCRE::3UTR (25 ng/ul), Punc-122::RFP] Line 2</i>	This paper	DCR Lab Strain ID: DCR5028
<i>C. elegans</i> : Strain DCR5029: <i>inx-1(ola278) X; olaEx2978 [Pcex-1::nCRE::3UTR (25 ng/ul), Punc-122::RFP] Line 3</i>	This paper	DCR Lab Strain ID: DCR5029

(Continued on next page)

Continued

REAGENT or RESOURCE	SOURCE	IDENTIFIER
<i>C. elegans</i> : Strain DCR5030: <i>inx-1(ola278) X; olaEx2979 [Podr-2b3a::nCRE (25 ng/ul), Punc-122::RFP] Line 1</i>	This paper	DCR Lab Strain ID: DCR5030
<i>C. elegans</i> : Strain DCR5031: <i>inx-1(ola278) X; olaEx2980 [Podr-2b3a::nCRE (25 ng/ul), Punc-122::RFP] Line 2</i>	This paper	DCR Lab Strain ID: DCR5031
<i>C. elegans</i> : Strain DCR5032: <i>inx-1(ola278) X; olaEx2981 [Podr-2b3a::nCRE (25 ng/ul), Punc-122::RFP] Line 3</i>	This paper	DCR Lab Strain ID: DCR5032
<i>C. elegans</i> : Strain DCR5035: <i>inx-1(ola278) X; olaex2984 [Ptx-3::SL2::nCRE::3UTR (25ng/ml), Punc122::RFP] Line 1</i>	This paper	DCR Lab Strain ID: DCR5035
<i>C. elegans</i> : Strain DCR5036: <i>inx-1(ola278) X; olaex2985 [Ptx-3::SL2::nCRE::3UTR (25ng/ml), Punc122::RFP] Line 2</i>	This paper	DCR Lab Strain ID: DCR5036
<i>C. elegans</i> : Strain DCR5037: <i>inx-1(ola278) X; olaex2986 [Ptx-3::SL2::nCRE::3UTR (25ng/ml), Punc122::RFP] Line 3</i>	This paper	DCR Lab Strain ID: DCR5037
<i>C. elegans</i> : Strain DCR4987: <i>Inx-1(ola278); olaEx2946 [Posm-6::nCRE::UTR (25ng/mL); Punc122::RFP] Line 1</i>	This paper	DCR Lab Strain ID: DCR54987
<i>C. elegans</i> : Strain DCR4988: <i>Inx-1(ola278); olaEx2947 [Posm-6::nCRE::UTR (25ng/mL); Punc122::RFP] Line 2</i>	This paper	DCR Lab Strain ID: DCR4988
<i>C. elegans</i> : Strain DCR4989: <i>Inx-1(ola278); olaEx2948 [Posm-6::nCRE::UTR (25ng/mL); Punc122::RFP] Line 3</i>	This paper	DCR Lab Strain ID: DCR4989
<i>C. elegans</i> : Strain DCR5108: <i>inx-1(ola278) X; olaEx3041 [Pceh-16::nCRE::3UTR, Punc-122::RFP] Line 1</i>	This paper	DCR Lab Strain ID: DCR5108
<i>C. elegans</i> : Strain DCR5109: <i>inx-1(ola278) X; olaEx3042 [Pceh-16::nCRE::3UTR, Punc-122::RFP] Line 2</i>	This paper	DCR Lab Strain ID: DCR5109
<i>C. elegans</i> : Strain DCR3056: <i>ola17 [Pmod-1::GCAMP6s (25ng/ul), Ptx-3::mCherry (25ng/ul), Punc-122::dsRed (40ng/ul)] I</i>	Hawk et al. ⁷⁰	DCR Lab Strain ID: DCR3056
<i>C. elegans</i> : Strain DCR5438: <i>ola17 [Pmod-1::GCAMP6s (25ng/ul), Ptx-3::mCherry (25ng/ul), Punc-122::dsRed (40ng/ul)] I; inx-1(gk580946) X</i>	This paper	DCR Lab Strain ID: DCR5438
<i>C. elegans</i> : Strain DCR9642: <i>inx-1(tm3524) X; olaEx5669[Ptx-3::GFP; Punc122::GFP] Line 4</i>	This paper	DCR Lab Strain ID: DCR9642
<i>C. elegans</i> : Strain DCR9646: <i>olaEx5669 [Ptx-3::GFP; Punc122::GFP] Line 4</i>	This paper	DCR Lab Strain ID: DCR9646
<i>C. elegans</i> : Strain DCR9643: <i>inx-1(tm3524) X; olals72 [Pelt-7::mCherry; Ptx-3G::SL2::CX36::mCherry]; olaEx5670 [Ptx-3::GFP; Punc122::GFP] Line 1</i>	This paper	DCR Lab Strain ID: DCR9643
<i>C. elegans</i> : Strain DCR8947: <i>inx-1(tm3524) X; olaEx5356[Ptx-3G::SL2::Cx36::mCherry (25ng/ul), Pelt-7::mCherry (25ng/ul)]</i>	This paper	DCR8947
<i>C. elegans</i> : Strain DCR4466: <i>ola17 [Pmod-1::GCAMP6s (25ng/ul), Ptx-3::mCherry (25ng/ul), Punc-122::dsRed (40ng/ul)] I; inx-1(tm3524) X</i>	This paper	DCR Lab Strain ID: DCR4466
Oligonucleotides		
See Table S1 in the supplemental information document for the complete list	This paper	N/A
Recombinant DNA		
Plasmid: DACR2397: Ptx-3G::sl2::CX36::mCherry	Hawk et al. ⁷⁰	DCR Lab Plasmid ID: DACR2397
Plasmid: DACR2217: Pceh-16::nCRE::unc54UTR	This paper	DCR Lab Plasmid ID: DACR2217
Plasmid: DACR2206: Pceh-1::nCRE::unc54UTR	This paper	DCR Lab Plasmid ID: DACR2206
Plasmid: DACR2194: Podr2b3a::nCRE::unc54UTR	This paper	DCR Lab Plasmid ID: DACR2194
Plasmid: DACR2188: Posm-6::nCRE::unc54UTR	This paper	DCR Lab Plasmid ID: DACR2188
Plasmid: DACR2186: Ptx-3::SL2::nCRE::unc54UTR	This paper	DCR Lab Plasmid ID: DACR2186
Plasmid: DACR2193: Pinx-1(1kb)::nCRE::unc54UTR	This paper	DCR Lab Plasmid ID: DACR2193
Plasmid: DACR2192: Pinx-1(2.5)::nCRE::unc54UTR	This paper	DCR Lab Plasmid ID: DACR2192

(Continued on next page)

Continued

REAGENT or RESOURCE	SOURCE	IDENTIFIER
Plasmid: DACR1605: Pinx-1:INX1gene:SL2:GFP	This paper	DCR Lab Plasmid ID: DACR1605
Plasmid: DACR1815: Pmod-1:INX-1B:unc54 3UTR	This paper	DCR Lab Plasmid ID: DACR1815
Plasmid: DACR1816: Pmod-1:INX-1A:unc54 3UTR	This paper	DCR Lab Plasmid ID: DACR1816
Software and algorithms		
Magat Analyzer Software Package	Gershov et al. ⁹⁴	N/A
LabView 2011	National Instruments	www.ni.com/en.html?cid=PSEA-7013q000001fLKAAA2-CONS-Bing_1239149829979437&utm_keyword=national%20instruments&msclkid=ab7b918cdac01b423c37f716bfc82087
MATLAB R2023a	Mathworks	www.mathworks.com/products/matlab.html
Time in isothermal tracking quantification Matlab code: GitHub: https://doi.org/10.5281/zenodo.14170612	This paper	https://github.com/colonramoslab/Almoril-Porras-et-al.-2023-Inx-1-14170612
Run duration quantification code for dispersion analysis Matlab code: GitHub: https://doi.org/10.5281/zenodo.14170612	This paper	https://github.com/colonramoslab/Almoril-Porras-et-al.-2023-Inx-1-14170612
General behavior cuantification matlab code: GitHub: https://doi.org/10.5281/zenodo.14170612	This paper	https://github.com/colonramoslab/Almoril-Porras-et-al.-2023-Inx-1-14170612
Time to reach isothermal tracking region Python code: GitHub: https://doi.org/10.5281/zenodo.14170612	This paper	https://github.com/colonramoslab/Almoril-Porras-et-al.-2023-Inx-1-14170612
Calcium Imaging Analysis Python code: GitHub: https://doi.org/10.5281/zenodo.14170612	This paper	https://github.com/colonramoslab/Almoril-Porras-et-al.-2023-Inx-1-14170612
Python	Python Software Foundation	www.python.org/
Prism	Graphpad Software Inc	https://www.graphpad.com/
Adobe	Adobe	https://www.adobe.com/products/illustrator.html
Fiji	Schindelin et al. ⁹⁵	https://imagej.net/Fiji/Downloads
TrackMate	Ershov et al. ⁹⁶	www.imagej.net/plugins/trackmate/
NIS-ELEMENTS	Nikon	www.microscope.healthcare.nikon.com/products/software/nis-elements
MicroManager	Edelstein et al. ⁹⁷	www.micro-manager.org
Clampex	Molecular Devices	www.moleculardevices.com/products/axon-patch-clamp-system/acquisition-and-analysis-software/pclamp-software-suite
Other		
MightEx BCE-B050-U	Mightex	www.mightexbio.com
Leica DM5500	Leica Microsystems	www.leica-microsystems.com
Leica DM6B	Leica Microsystems	www.leica-microsystems.com
Hamamatsu ORCA-FUSIONBT SCMOS	Haamamatsu	https://www.hamamatsu.com/jp/en/product/cameras/cmos-cameras/C15440-20UP.html
confocal spinning disk CSU-W1 System	Yokogawa	https://www.yokogawa.com/solutions/products-and-services/life-science/spinning-disk-confocal/csu-w1-confocal-scanner-unit/
CFI PLAN APO LAMBDA 60X OIL objective	Nikon	https://www.microscope.healthcare.nikon.com/products/optics/cfi-plan-apochromat-lambda-series
Nikon Ti2-E Inverted Microscope	Nikon	www.microscope.healthcare.nikon.com/
dPatch Low-Noise Ultra-Fast Digital Patch Clamp Amplifier System	Sutter Instrument	www.sutter.com/AMPLIFIERS/dpa.html

(Continued on next page)

Continued

REAGENT or RESOURCE	SOURCE	IDENTIFIER
iXonEM + 885 Electron Multiplying CCD camera	Oxford Instruments	andor.oxinst.com/products/ixon-emccd-cameras-for-life-science
59222 ET filter set	Chroma Technology Corp.	www.chroma.com/products/sets/59222-et-egfp-mcherry-or-fitc-txred-with-single-band-exciters
Light Source	Sutter Instrument	sutter.com/IMAGING/lambdaxl_frame.html
Multiclamp 700B amplifier	Molecular Devices	www.moleculardevices.com/products/axon-patch-clamp-system/amplifiers/axon-instruments-patch-clamp-amplifiers
Axon Digidata 1550B Low-Noise Data Acquisition System plus HumSilencer	Molecular Devices	www.moleculardevices.com/products/axon-patch-clamp-system/digitizers/axon-digidata-1550b-plus-humsilencer
Nikon FN-1	Nikon	www.microscope.healthcare.nikon.com/products/upright-microscopes/eclipse-fn1

EXPERIMENTAL MODEL AND STUDY PARTICIPANT DETAILS**C. elegans**

Nematodes were regularly maintained at room temperature (20–23°C) or inside Precision 815 (Thermo Scientific) or I-36NL (Percival Scientific) incubators at 20°C, grown on bacterial lawns of *Escherichia coli* strain OP50 seeded onto Nematode Growth Medium, according to husbandry standards.⁹⁸ One-day adult hermaphrodite worms were used in all experiments unless otherwise noted. The N2 Bristol strain was used as the wild-type background. See the [key resources table](#) for a complete list of the strains used in this study.

METHOD DETAILS**Molecular biology**

Plasmids were generated using Gibson Assembly (New England Biolabs) or the multi-site Gateway cloning system (Invitrogen). Either Phusion or Q5 High-Fidelity DNA-polymerase (NEB) were used for cloning or subcloning elements into the Gateway entry vectors. Cell-specific promoter fragments were amplified from genomic DNA or preexisting plasmids and introduced into pENTR41 or pENTR 50-TOPO vectors (Invitrogen); CDS of interest were inserted into pDONR221[1-2] (Invitrogen); and preexisting 3'UTR regions of commonly used genes (*unc-54*, *let-858*) into pDONR221[2-3] were used. Every insert was sequenced in their respective entry vector prior to the four-component LR recombination to generate the final expression plasmid.⁹⁹

Nematode Strains and maintenance

Nematodes were regularly maintained at room temperature (20–23°C) or inside Precision 815 (Thermo Scientific) or I-36NL (Percival Scientific) incubators at 20°C, grown on bacterial lawns of *Escherichia coli* strain OP50 seeded onto Nematode Growth Medium, according to husbandry standards.⁹⁸ One-day adult hermaphrodite worms were used in all experiments unless otherwise noted. The N2 Bristol strain was used as the wild-type background.

Genotyping of mutant strains

Adult worms were lysed following standard protocols and PCRs were performed using GoTaq Green Master Mix (Promega, REF-M7123). Mutant alleles were distinguished from wild type by imaging Restriction Fragment Length Polymorphisms (RFLP) on an agarose gel or by Sanger Sequencing performed by GENEWIZ (Azena Life Sciences). The full set of genotyping primers can be found in the [key resources table](#), and [supplemental information](#) sections.

For genotyping the *inx-1(tm3524)* X allele, the annealing temperature was 55°C, and elongation 1 minute at 72°C. Amplified products were run on a 2% agarose gel. Homozygous wild type produces 542bp & 159bp bands, while homozygous *inx-1(tm3524)* X produces a single 304bp band, and a heterozygous *inx-1(+/tm3524)* X will produce three bands at 542bp, 304bp & 159bp.

For *inx-1* exome sequencing, annealing temperature was 55°C, elongation time 1 minute and 15 seconds at 72°C. Resulting products were sent out for Sanger Sequencing performed by GENEWIZ (Azena Life Sciences). Products are 576bp, 982bp, 994bp and 250bp for each respective exome primer sets.

Generation of transgenic strains

Transgenic *C. elegans* strains were generated by microinjection of the plasmids of interest into the gonad syncytia following standard approaches.¹⁰⁰ Transgenic lines were selected and maintained based on the expression of one or multiple of the following

co-injection markers: *Punc-122::GFP*, *Punc-122::RFP*, *Punc-122::dsRed Pmyo-3::mCherry*, *Pelt-7::GFP::NLS* or *Pelt-7::mCherry::NLS*. Extrachromosomal arrays were integrated into the nematode genome via UV-activated trimethylpsoralen (TMP, Sigma, T6137), following standard methods. For a full list of strains used and generated by this work, please refer to [key resources table](#).

Sensitized forward-genetic screens

To unbiasedly find new genes that might regulate or modulate the distinct thermotaxis gradient migration and isothermal tracking behaviors, forward-genetic screens were performed on *pkc-1(nj1)* loss-of-function mutants (strain *IK105* in [key resources table](#)), which perform constitutively thermophilic behaviors. This screen resulted in recovery of *ola375*. In addition to suppressing the *pkc-1(nj1)* mutant phenotype of migrating up a shallow temperature gradient regardless of their preferred trained temperature,¹⁰¹ these animals tracked isotherms more often, and further away from their preferred temperature. We mapped the causative lesion to a 5 Mb region in Chromosome X (genomic position ~3Mb to ~8Mb) by Hawaiian SNP mapping⁴³ and Whole-Genome Sequencing (WGS)^{44,45} making use of the CloudMap pipeline.⁴⁶ Whole-Genome Sequencing (WGS) was performed by the Yale Center for Genome Analysis (YCGA).

Identification of *ola375* causative lesions

We further characterized the causative molecular lesion of *ola375* by fine mapping using SNPs present in the divergent, Hawaiian wild-type strain (CB4856)⁴³ and outcrossing SNPs with the reference N2 wild-type strain. When recombinants with wild-type DNA regions within the 5Mb previously-mapped region were recovered, from either the 3Mb or the 8Mb flank, both the suppressing *pkc-1(nj1)* phenotype and the isothermal “hypertracking” phenotype were greatly diminished. Further analysis of the behavioral phenotypes, in combination with underlying molecular lesions in that region, led us to identify a mutant allele for gap junction innexin gene *inx-1(ola375)*, which was exclusively responsible for the isothermal “hypertracking” phenotype under a wild-type background. This genetic lesion consists on both a missense SNP and a small indel in the fifth coding exon, resulting in an early STOP codon (see [Figure 1D](#); [Figure S1](#); [supplemental information](#)). We established that *inx-1(ola375)* is the causative lesion to the isothermal tracking defects detected in this screen via four approaches: 1) examining additional alleles of *inx-1*, namely *tm3524* and *gk580946*, and determining that they phenocopy the behavioral phenotypes (persistent isothermal tracking) observed for *inx-1(ola375)*; 2) performing complementation tests to allele *tm3524* and determining that *inx-1(ola375)* fails to completement the observed behavioral phenotypes; 3) performing genetic rescue experiments with a genomic region of *inx-1* and observing that is sufficient to rescue the behavioral phenotypes and 4) performing conditional knock-out experiments and observing that cell-specific knockouts of *inx-1* in the AIY interneurons are sufficient to reconstitute the observed behavioral phenotype for *inx-1(ola375)*.

Generation of “floxed” *inx-1(ola278)* for conditional Knock-Out experiments

We inserted *LoxP* sites flanking the endogenous *inx-1* genomic coding locus via the CRISPR-based, genomic edition protocol detailed in Dickinson et al.⁶⁸ This strain also carries an inserted *tagRFP* sequence and a *Hygromycin B* resistance gene after the 3' *LoxP* insertion ([Figure S1F](#)). Complete inserted sequence can be found in [Data S1](#).

Complementation Assays

To obtain *inx-1(tm3524)/ola375* transheterozygous animals, *inx-1(tm3524)* males that have coelomocytes tagged with GFP (see [key resources table](#)) were crossed with *ola375* hermaphrodites. From the progeny, hermaphrodites possessing the marker were picked in L4 stage for running behavioral assays at 0.8 °C/cm gradient.

Thermotaxis Behavioral Assays

For all behavior experiments, the animals' developmental stage was synchronized by either allowing gravid adults to lay eggs in a seeded plate for two hours, three days prior to the assay or by picking L4 animals – identified by the clear half-moon patch in the midsection of the animal – the day before the experiment. The plates were then kept in Precision 815 (Thermo Scientific) or I-36NL (Percival Scientific) incubators at 20°C up to the time of the experiment for experiments with a cultivation temperature of 20°C, or shifted to the appropriate temperature 4-6 hours prior to testing, in the case of temperature shift assays. Behavioral analyses were performed as described previously.^{42,70} A population of synchronized one-day adult hermaphrodites were picked onto an unseeded plate and washed in M9.¹⁰² 3-5 worms were then transferred by micropipette on a 3µl M9 droplet to the respective starting points on the assay plates,¹⁰³ equilibrated for 5-10 min, and they were allowed to freely crawl on the arena for 30-60 min, acquiring images at 2fps with a MightEx BCE-B050-U camera. Nematode tracks were identified from the collected images using the MagatAnalyzer software package with modifications as previously indicated.^{42,70,94}

Shallow gradients for Gradient Migration Quantification

The original suppressor screen was performed on equipment previously described,^{42,70} monitoring nematode gradient migration in the presence of a shallow temperature gradient (0.18°C/cm). Briefly, two pairs of thermoelectric components controlled by two Ac-cuthermo FTC100D PID controllers sit at either side of an aluminum slab, and generate a defined linear temperature gradient. The system is cooled by a closed refrigeration system connected to a liquid cooling radiator in contact with dry ice. The aluminum slab in turn contacts a square assay plate (Corning®) with a 224 x 224 mm internal arena where the worms will perform. To ensure

efficient heat transfer between the slab and the arena, either a volume of glycerol was used, or a fitted smaller aluminum sheet was intercalated between the aluminum slab and the assay plate. Red LEDs parallel to the plate generate a dark background image with bright outlines of the nematodes, captured by a MightEx camera (BCE-B050-U) above, at 2 frames per second, for 30–60 min. The whole system is encased in a modified cabinet. Unless otherwise explicitly noted, the gradient of the arena goes from 18°C to 22°C, and animals are placed in the middle of the arena, near 20°C. 24–33 animals are tested per assay.

Moderate and steep gradients for Isothermal Tracking Quantification

C. elegans perform maximal isothermal tracking behavior at ~0.6°C/cm gradients or higher.²² To generate these gradients, we used a modified, smaller version of the equipment described above and previously,^{42,70} kindly gifted to us by Aravi Samuel (Harvard University). Unless otherwise explicitly noted, the gradient on the arena is centered on 20°C and goes from 17°C to 23°C for 0.6°C/cm gradient and 16°C to 24°C for 0.8°C/cm gradient. For the classical assay placement, 9 animals in 3 droplets were placed along the 20C isothermal line in the middle of the arena. To quantitatively assess and adequately quantify isothermal tracking across the full gradient, a population of animals is assayed by starting in an H configuration, as shown in Figures 1F and 1G (yellow start sites). The “H-format” assay was intentionally developed to examine the choices of animals performing isotherms when they are placed above, below or at T_c for the examined genotypes. For an assessment of animals performing more isothermal tracking or under the wrong context, four starting droplets at each respective edge of the gradient were used. 24–27 animals are tested per assay.

Dispersion Assays

L4 stage hermaphrodites were picked into a plate seeded with *E. coli* the day before the experiment, and kept overnight at 20°C. No less than 1 hour before the experiment, the plates were placed next to the assay arena to acclimate animals to ambient temperature. Unlike for thermotaxis assays, in dispersion the heating and cooling units were turned off to not generate a predetermined temperature gradient. Animals were then washed in M9 buffer and onto an unseeded plate, and transferred into the 22x22cm agarose arena in 3µL droplets, each with approximately 3 animals. Animals were distributed in the arena as to avoid collisions (in the top left, bottom left, center, top right and bottom right areas of the arena). Acquisition started no less than 10mins after placing the last droplet.

Confocal imaging

Young adults or L4 hermaphrodite animals were mounted in 2% agarose dissolved in M9 buffer pads and anaesthetized with 10mM levamisole (Sigma). Confocal images were acquired with dual Hamamatsu ORCA-FUSIONBT SC莫斯 cameras on a Nikon Ti2-E Inverted Microscope using a confocal spinning disk CSU-W1 System, 488nm and 561nm laser lines and a CFI PLAN APO LAMBDA 60X OIL objective. Images were captured using the NIS-ELEMENTS software, with 2048px x 2048px, 16-bit depth, 300nm step size, 300ms of exposure time and enough sections to cover the whole worm depth.

Calcium Imaging

Imaging calcium dynamics was performed as previously described,⁷⁰ with some modifications. The sample mounting protocol was modified to enrich the samples with animals positioned dorsoventrally, allowing for imaging of both AIY neurons simultaneously. Temperature control elements and most microscopy elements remain identical to Hawk et al.,⁷⁰ with a Leica DM6B being used in addition of Leica DM5500. Image acquisition was performed using MicroManager.⁹⁷ For imaging calcium dynamics, the imaging pad was first made by placing 5% Agarose dissolved in M9 buffer unto a 22x22mm glass slide and pressing it with a larger 25x75cm microscope slide. 18µl Levamisole was then placed on top of the pad. Using a minimal amount of bacteria, worms were picked from their respective cultivation plate, onto one without bacteria, removing excess bacteria afterwards. It was then flooded with M9 buffer, then pipetted as many as possible in 2 droplets of 3µl into the imaging pad. The levamisole, M9 buffer, and NGM plate without bacteria were maintained at cultivation temperature of 20C. To enrich for dorsoventral view, a 5mins rest time was given before proceeding. Any excess liquid remaining was removed by slightly tilting the coverslip while keeping the worms uphill, and then removing the excess on the bottom by cutting that part of the pad. The worms were grouped together using an eyelash pick. Once the pad is almost dry, the top coverslip was carefully placed. The imaging pad was then moved to the temperature stage, previously set to constant 20C, while the image was focused to start acquisition.

The temperature stage consists of a black painted Peltier plate surface. A cooling system removing excess heat runs through a copper cooling block attached to the bottom surface of the stage. Temperature was controlled through custom LabView (National Instruments) software and H-bridge amplifier (Accuthermo FTxD700D) and controller (Accuthermo FTC200), that obtain temperature measurements from a thermal probe (Omega SRTD-2). Micromanager⁹⁷ was used to acquire fluorescence images over time at 250ms exposure time, 1fps and 1x1 binning. A Leica DM5500 and Leica DM6B microscope with a 10XX/0.40 HC PL APO air objective, Photometrics Dual-View 2 (DV2) optical splitter and Hamamatsu ORCA-Flash 4.0 LT camera were used to acquire images with both green and red channels.

Electrophysiological experiment and analyses

The electrophysiological experiments involving calcium imaging of AIY neurons were conducted using transgenic strains expressing *Pmod-1::GCaMP6s* and *Ptx-3::mCherry*, in both wild type and *inx-1(gk580946)* mutants. Experiments performed for measuring AIY membrane resistance, membrane capacitance and membrane voltage response to current injections were conducted in transgenic

strains expressing *Ptx-3G::GFP* in wild type and *inx-1(tm3524)* mutants. In each experiment, a young adult hermaphrodite animal was immobilized on a Sylgard-coated circular coverglass by applying Vettbond Tissue Adhesive (3M Company) along the anterior dorsal region. A longitudinal cut (~ 200 µm) was made by a diamond dissecting tool in the glued area. The cuticle above the cut was gently pulled back and affixed to the coverglass, exposing head neurons. The coverglass was then placed in a recording chamber filled with extracellular solution (composition: NaCl 140 mM, KCl 5 mM, CaCl₂ 5 mM, MgCl₂ 5 mM, dextrose 11 mM and HEPES 5 mM, pH 7.2). The pipette solution contained (in mM) KCl 120, KOH 20, Tris 5, CaCl₂ 0.25, MgCl₂ 4, sucrose 36, EGTA 5 and Na₂ATP 4 (pH 7.2). The two AIYs were identified based on either mCherry or GFP fluorescence, and one of them was patch-clamped to establish the classical whole-cell configuration.

Since this study represents, to our knowledge, the first-time information about gap junction function in *C. elegans* has been obtained based on the voltage clamp of a single neuron, we implemented a new system (dPatch-2, Sutter Instruments) and methodologies that were optimized in collaboration with technical staff from Sutter Instruments towards measurements of membrane resistance and membrane capacitance of very small cells (like *C. elegans* neurons). Membrane capacitance and resistance were determined using the Membrane Test function of a dPatch-2 digital patch clamp amplifier system (Sutter Instruments). In voltage-clamp experiments for assessing membrane depolarization on calcium signals, one AIY was stepped from -60 mV to +40 mV for 20 seconds before returning to -60 mV. Calcium transients of both AIYs were imaged before (10 sec), during (20 sec), and after (30 sec) the voltage step at 1-second intervals using an electron-multiplying CCD camera (iXonEMp885, Andor Technology), a FITC filter set (59222, Chroma Technology Corp.), a light source (Lambda XL, Sutter Instrument), and NIS-Elements software (Nikon). TTL signals from the camera synchronized the recordings of calcium transients with the voltage-clamp protocol. In current-clamp experiments for assessing the effect of current injections on membrane voltage, negative and positive currents ranging from -10 pA to +20 pA at 2.5-pA intervals were injected into a clamped AIY for 5 seconds per step. Except for the voltage-clamp experiments for measuring membrane capacitance and membrane resistance, all electrophysiological experiments were conducted using a Multiclick 700B amplifier (Molecular Devices, Sunnyvale, CA), a digitizer (Digidata 1550B, Molecular Devices), and Clampex software (version 11, Molecular Devices) with data filtered at 2 kHz and sampled 10 kHz. The voltage-clamp experiments for measuring membrane resistance and membrane capacitance were conducted using a digital patch clamp amplifier system (d-Patch-2, Sutter Instrument). Borosilicate glass pipettes with a tip resistance of approximately 20 MΩ were used as electrodes in all electrophysiological recordings. The electrophysiological and calcium imaging experiments utilized a Nikon FN-1 microscope equipped with a 40X water immersion objective, an electron-multiplying CCD camera (iXonEM+885, Andor Technology), a light source (Lambda XL, Sutter Instrument) with a filter wheel, and the NIS-Elements software (Nikon).

QUANTIFICATION AND STATISTICAL ANALYSIS

Statistical Tests

Statistical tests of dispersion assay results were performed using Python version 3.11, Python Software Foundation, www.python.org. All other statistical tests were performed using GraphPad Prism version 9 for Windows, GraphPad Software, San Diego, California USA, www.graphpad.com. Chosen statistical tests are described in the relevant figure legends. All the codes used in the study can be accessed at the following repository: GitHub: <https://doi.org/10.5281/zenodo.14170612>.

Quantification of isothermal tracking

Worm tracks were first analyzed and segmented by a modified MAGATAnalyzer software package.^{42,94} These trajectories were then filtered into periods of isothermal tracking, defined as forward motion events in which at least 90% of the displacement occurred in the vertical, isotherm orientation, for a minimum of 25 seconds; and periods of non-isothermal tracking in which the movement of the worm did not pass the isothermal tracking filter. The segmented isothermal tracking periods were further analyzed by their duration in seconds, temperature at which the period started and number of events.

Quantification of behavior

Quantifications of turns, thermotaxis indices and other parameters relevant to gradient migration were automatically scored per worm track by an adapted MAGATAnalyzer software package, previously described.^{42,94} For dispersion assays, worm tracks were first analyzed and segmented by the same modified MAGATAnalyzer software package. Then in custom MATLAB scripts trajectories movements were filtered into 2 categories: runs, which are defined as forward motion events where the direction of travel does not change abruptly by more than 25 degrees, and is sustained for at least 22.5 seconds; and other forms of movements like turns. We note that using other parameters similar results. Statistical analysis and plotting were done on python. All codes used in the study can be accessed at GitHub: <https://doi.org/10.5281/zenodo.14170612>.

The time taken to reach the isothermal tracking region (14°C for the 0.8°C/cm gradient going from 16°C to 24°C) was obtained by identifying the time point corresponding to when the X coordinates for the tracks first registered to reach or pass the positional coordinate pertaining to 14°C. Tracks that, within the experimental time of 1 hour, never met this criteria were not included in the average and analysis. This procedure was coded in Python.

Quantification of calcium imaging in AIY

FIJI⁹⁵ with TrackMate⁹⁶ plugin were used to define the portion of each AIY at zone 2 as regions of interest, track over time and calculate the intensities. Tracking was done with the semiautomatic tracking feature. Downstream processing was done with custom Python scripts, which includes alignment of intensities with temperature, response detection and heatmap generation. Responses were scored as the initial rise of the AIY calcium signal as determined by an automated response calling based on signal intensity and its derivative.

Supplemental figures

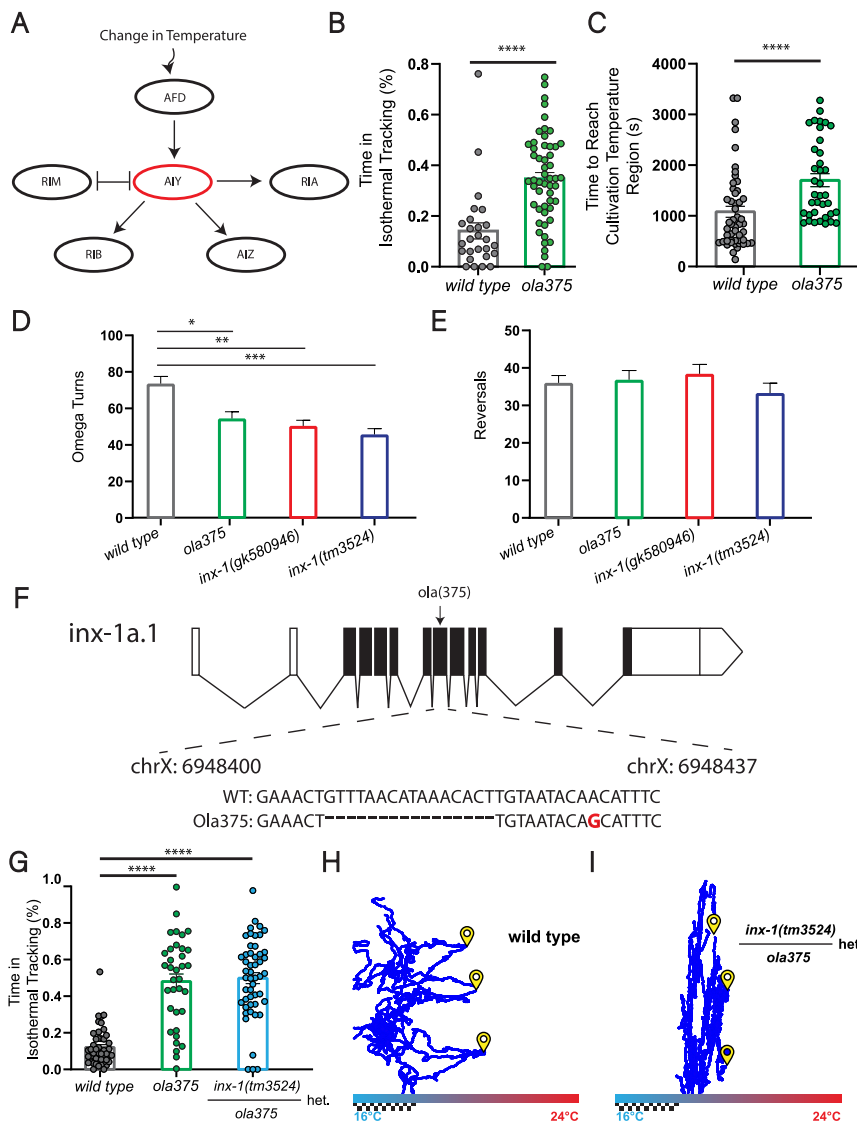


Figure S1. Strategies, strains, and quantifications, related to Figure 1

(A) Schematic of the core part of the thermotaxis circuit. All neurons outlined here are bilaterally symmetric. Sensory neuron AFD is the main thermosensory neuron of the circuit,^{23,33,34,104} and its only known chemical synaptic outputs are onto interneuron AIY.³² AIY also receives chemical synaptic outputs from other sensory neurons and interneurons (not shown in this schematic), and it forms presynaptic specializations primarily onto interneurons AIZ, RIA, and RIB. AIY is also known to form electrical synapses onto motor interneuron RIM.³²

(B) Percentage of total time animals spend tracking isotherms (per worm track, which includes in the denominator the time spent performing gradient migration) for wild type and ola375 mutants in experiments corresponding to Figures 1B and 1C. Individual track values are presented by single-colored dots, $n = 26$ and 53 tracks over multiple experiments for wild type and ola375, respectively. Colors denote genotypes. Values are shown as mean \pm SE and *** denotes $p < 0.0001$ by two-tailed Mann-Whitney test.

(C) Average time to reach the cultivation temperature region ($\pm 2^\circ\text{C}$). Individual track values are presented as single-colored dots. $n = 50$ tracks for wild type and 37 tracks for ola375. Values are shown as mean \pm SE. Colors denote genotypes and *** $p < 0.0001$ by two-tailed Mann-Whitney test.

(D) Number of omega turns, in data presented in Figure 1B. *, **, and *** denote $p < 0.05$, $p < 0.01$, and $p < 0.001$, respectively. Values are shown as mean \pm SE and colors denote genotypes.

(E) As in (D), but the number of reversals. Statistics by Dunn's multiple comparisons test following a Kruskal-Wallis test.

(legend continued on next page)

-
- (F) Schematic and sequence information for the *inx-1(ola375)* allele isolated in this study from forward-genetic screens.
- (G) Complementation test between allele *ola375* and *inx-1(tm3524)* (by building transheterozygote *inx-1(tm3524/ola375)*) and as quantified by the percentage of total time spent in isothermal tracking behavior. Individual track values are presented by single-colored dots, where $n = 46$ (wild-type tracks), $n = 50$ (transheterozygote tracks), and $n = 35$ (*ola375* tracks). Bars represent mean \pm SE and *** denotes $p < 0.0001$ by Dunn's multiple comparisons test following a Kruskal-Wallis test. Colors denote genotypes. Note how the transheterozygote allele *inx-1(tm3524/ola375)* displays the same mutant phenotype as the homozygote *ola375* allele, indicating that it fails to complement the phenotype, consistent with the phenotypes in *ola375* corresponding to a genetic lesion in the *inx-1* gene (in F).
- (H) Tracks of wild-type animals trained to prefer 15°C. Animals start points denoted with yellow symbol.
- (I) As in (H), but for transheterozygote *inx-1(tm3524/ola375)* that was quantified in (G).

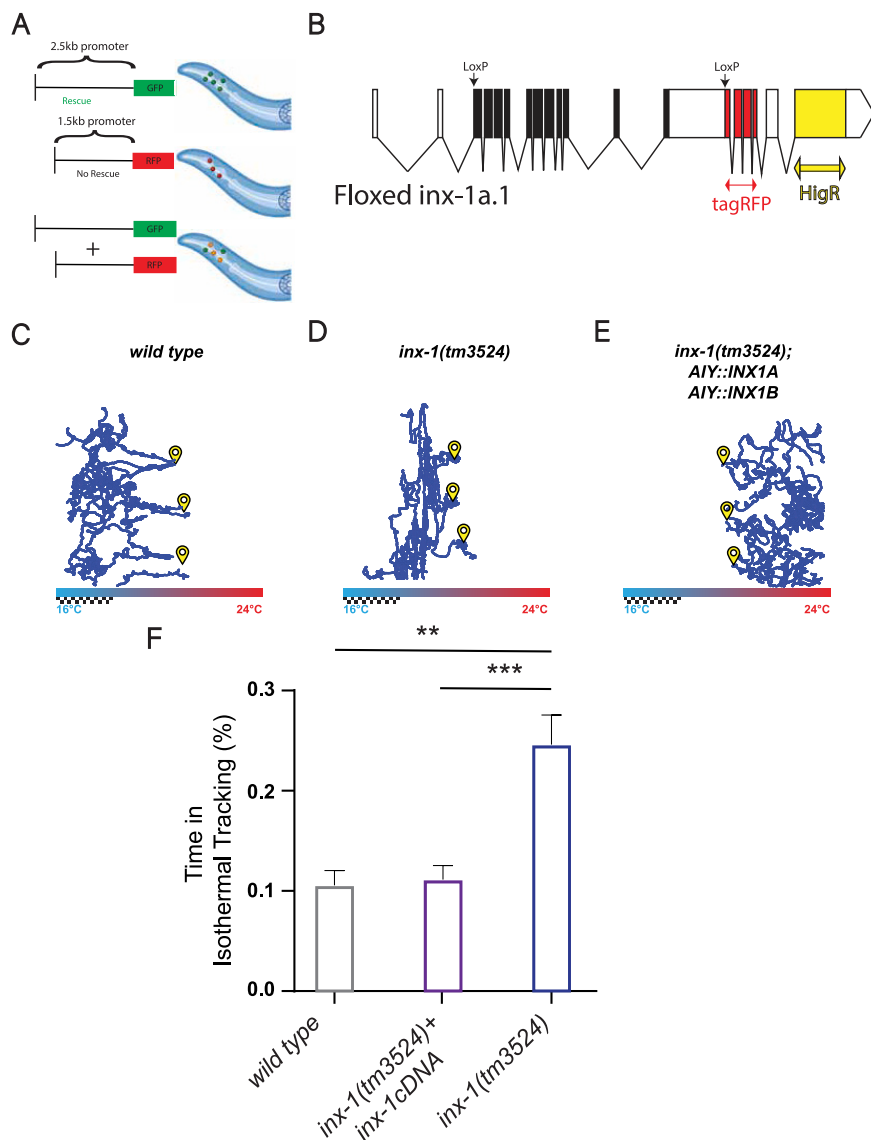


Figure S2. Examination of the site of action of INX-1 for the observed thermotaxis behavioral defects, related to Figure 2

(A) Schematic of the subtractive labeling strategy to identify the INX-1 site of action. A genomic fragment containing promoter fragment of 2.5 kb can drive expression of *inx-1* and rescue the observed thermotaxis defects for the *inx-1* mutants, while a promoter fragment of 1.5 kb is insufficient to do so. By creating transcriptional fusions of both promoter fragments, we identified candidate neurons that are uniquely labeled by the rescuing promoter fragment.

(B) Schematic of *inx-1(ola278)*, a floxed allele engineered for conditional knockdowns of the *inx-1* gene.

(C) Tracks of wild-type animals trained to prefer 15°C. Animals start points denoted with yellow symbol.

(D) As in (C), but for *inx-1(tm3524)* mutants.

(E) As in (C), but expressing the *inx-1* isoform A and isoform B cell specifically in AIY by using the *mod-1* promoter. Note how the expression of the cDNA of *inx-1* in AIY suppresses the isothermal tracking phenotype, but it also results in a gain-of-function phenotype of animals moving toward warmed temperatures under conditions in which they were trained to prefer 15°C (compare with C), also in Hawk et al.⁷⁰

(F) Percentage of total time isothermal tracking for the experiments shown in (C)–(E), where $n = 35$ (wild type), $n = 56$ (*inx-1(tm3524)* + *inx-1* cDNA in AIY), and $n = 37$ *inx-1(tm3524)* tracks over multiple experiments. ** and *** denote $p < 0.01$ and $p < 0.001$, respectively. Tested by Dunn's multiple comparisons test followed by Kruskal-Wallis test. Values are shown as mean \pm SE.

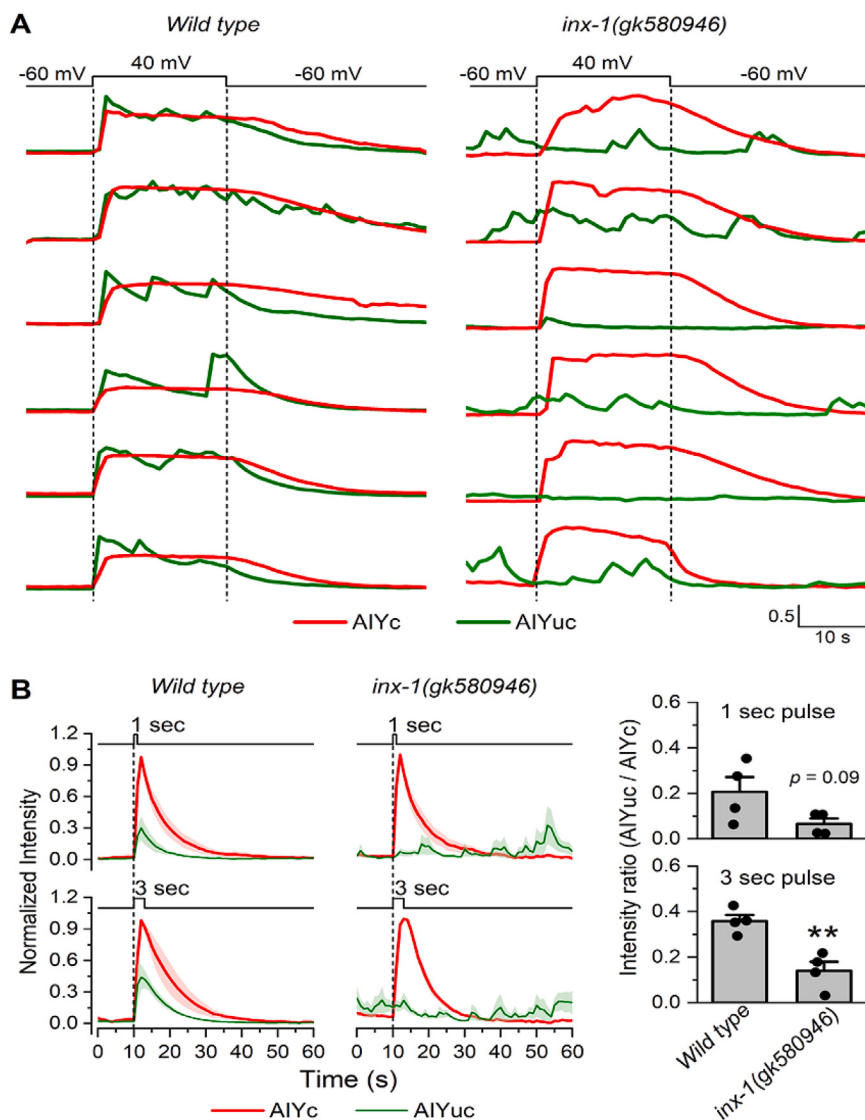


Figure S3. Examination of AIY coupling by INX-1, related to Figure 3

GCaMP6 signal strength over time in clamped AIY (AIY_c) and unclamped AIY (AIY_{uc}) of wild type (left) and the *inx-1* mutants (right). Shown here are results of individual animals normalized by the peak fluorescent signal of AIY_c.

(A) represents the individual traces used for Figure 3C.

(B) corresponds to stimuli with varying time lengths, as indicated, with comparative quantifications (similar to Figure 3D) in the graphs to the bottom right. Values are shown as mean \pm SE.

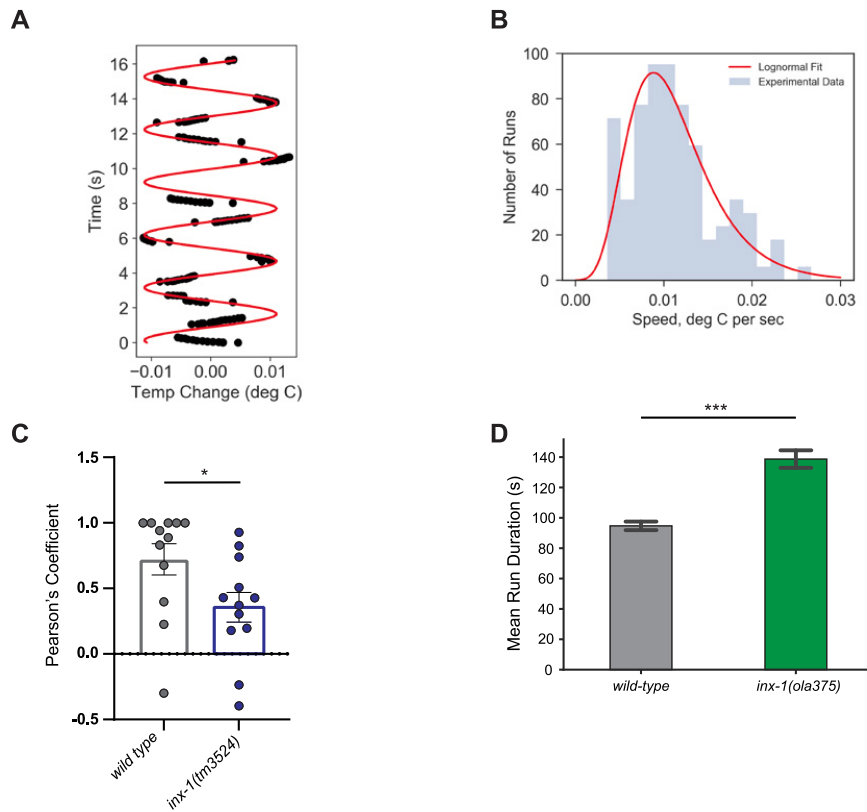


Figure S4. Thermotaxis modeling parameterization and Pearson coefficient correlation between AIY pairs, related to Figure 5

(A) Data from a freely moving animal during a run, displaying the position of the nose tip (dots) and fit with a sinusoidal curve.

(B) Histogram of the speeds of runs of animals trained at 25°C and placed at 20°C and moving up the gradient toward their preferred temperature, with a lognormal fit (in red).

(C) Pearson's coefficient in AIY pairs between wild-type animals ($n = 12$) and *inx-1(tm3524)* ($n = 12$). Values are shown as mean \pm SE. The asterisk * denotes $p < 0.05$ from two-tailed Mann-Whitney test.

(D) Mean run durations of *inx-1(ola375)* mutants and wild-type animals in dispersion assays. No less than 15 animals were analyzed per experiment, and a total of 3 assays were conducted for wild-type and various alleles of *inx-1* mutants, including *inx-1(gk580946)* and *inx-1(tm3524)* alleles, which similarly displayed significantly higher run duration as compared with wild type (wild-type run duration = 94.71 s, *inx-1(gk580946)* run duration = 113.92 s, and *inx-1(tm3524)* run duration = 119.96 s). Error bars are shown as \pm SE, and *** denotes $p < 0.001$, by two-tailed Mann-Whitney test.